




AKT2 reduces IFN β 1 production to modulate antiviral responses and systemic lupus erythematosus

Xin Zheng^{1,2}, Jun Xiao¹, Qi Jiang², Lingming Zheng¹, Chang Liu³, Chen Dong¹, Yuxiao Zheng¹, Peili Ni⁴, Chi Zhang^{1,2}, Fang Zhang^{3,5}, Ruiyue Zhong¹, Huihua Ding⁶, Qiong Wang⁵, Ying Qiu^{1,3}, Minxia Gao¹, Jianping Ding¹ , Nan Shen⁶, Bin Wei^{3,5,*}  & Hongyan Wang^{1,2,**} 

Abstract

Interferon regulatory factor 3 (IRF3)-induced type I interferon (I-IFN) production plays key roles in both antiviral and autoimmune responses. IRF3 phosphorylation, dimerization, and nuclear localization are needed for its activation and function, but the precise regulatory mechanisms remain to be explored. Here, we show that the serine/threonine kinase AKT2 interacts with IRF3 and phosphorylates it on Thr207, thereby attenuating IRF3 nuclear translocation in a 14-3-3 ϵ -dependent manner and reducing I-IFN production. We further find that AKT2 expression is downregulated in viral-infected macrophages or in monocytes and tissue samples from systemic lupus erythematosus (SLE) patients and mouse models. *Akt2*-deficient mice exhibit increased I-IFN induction and reduced mortality in response to viral infection, but aggravated severity of SLE. Overexpression of AKT2 kinase-inactive or IRF3-T207A mutants in zebrafish supports that AKT2 negatively regulates I-IFN production and antiviral response in a kinase-dependent manner. This negative role of AKT2 in IRF3-induced I-IFN production suggests that AKT2 may be therapeutically targeted to differentially regulate antiviral infection and SLE.

Keywords AKT2; I-IFN; IRF3; SLE; viral infection

Subject Categories Immunology; Microbiology, Virology & Host Pathogen Interaction

DOI 10.15252/embj.2021108016 | Received 13 February 2021 | Revised 2 December 2021 | Accepted 23 December 2021 | Published online 22 February 2022

The EMBO Journal (2022) 41: e108016

Introduction

I-IFN and IFN-induced transcription of a wide range of IFN-stimulated genes (ISGs) are both critical to elicit innate and adaptive immune responses against various infections (Sadler & Williams, 2008; Schneider *et al.*, 2014; Wu & Chen, 2014; Boxx & Cheng, 2016). However, I-IFN is pathogenic during the development of autoimmune disorders, which might be triggered by multiple genetic and environmental factors. Especially, the persistent presence of I-IFN has been proved to accelerate the pathogenesis of SLE (Munz *et al.*, 2009; Bengtsson & Ronnblom, 2017). It is therefore vital to understand the precise mechanism of regulating I-IFN production, which can offer new drug targets to treat infections or SLE.

The induction of I-IFN is elicited by pattern recognition receptors (PRRs) and a cascade of downstream molecules. IRF3 is a master transcription factor for I-IFN production, and IRF3 transcriptional activity and other biological functions are precisely regulated via its phosphorylation (Taniguchi *et al.*, 2001; Saitoh *et al.*, 2006; Chattopadhyay *et al.*, 2016; Huai *et al.*, 2019). Phosphorylated IRF3 undergoes conformational change to form dimers, which then enters the nuclei and associates with interferon transcriptional elements to initiate I-IFN transcription, mainly *Irfb1* (Honda *et al.*, 2006; Sadler & Williams, 2008). Phosphorylation sites of the cluster 1 (Ser385/Ser386) and the cluster 2 (Ser396, Ser398, Ser402, Thr404, and Ser405) in the C terminus of IRF3 have been demonstrated to indicate IRF3 activation status in antiviral immunity (Lin *et al.*, 1998, 1999; Panne *et al.*, 2007). Further studies suggest that Ser386 is critical, while Ser396 plays a moderate role in IRF3 dimerization and activation (Dalskov *et al.*, 2020; Jing *et al.*, 2020), and PTEN regulates the phosphorylation of IRF3 at Ser97 to prevent IRF3 nuclear import (Li *et al.*, 2016). Despite these findings, it is still unclear whether

1 State Key Laboratory of Cell Biology, Shanghai Institute of Biochemistry and Cell Biology, Center for Excellence in Molecular Cell Science, Chinese Academy of Sciences, University of Chinese Academy of Sciences, Shanghai, China

2 School of Life Science, Hangzhou Institute for Advanced Study, University of Chinese Academy of Sciences, Hangzhou, China

3 Cancer Center, Shanghai Tenth People's Hospital, School of Medicine, Tongji University, Shanghai, China

4 CAS Key Laboratory of Nutrition, Metabolism and Food Safety, Shanghai Institute of Nutrition and Health, Chinese Academy of Sciences, Shanghai, China

5 School of Life Sciences, Shanghai University, Shanghai, China

6 Shanghai Institute of Rheumatology, Renji Hospital, Shanghai Jiao Tong University School of Medicine (SJTUSM), Shanghai, China

*Corresponding author. Tel: +86 021 66130717; E-mail: weibinwhy@shu.edu.cn

**Corresponding author. Tel: +86 021 54921089; E-mail: hongyanwang@sibcb.ac.cn

IRF3 phosphorylation at other sites could affect the intracellular vs. nuclear translocation of IRF3.

The serine/threonine kinase AKT (also named protein kinase B/PKB) represents a critical kinase family that can phosphorylate different target proteins and control a variety of cellular functions. AKT family contains three highly conserved isoforms in mammals, AKT1/PKB α , AKT2/PKB β , AKT3/PKB γ (Fayard *et al.*, 2010). There are growing researches about the distinct role of AKTs in the induction of I-IFN. After herpes simplex virus-1 (HSV-1) infection, AKT1 phosphorylates TBK1 to attenuate STING signaling (Wu *et al.*, 2019); others also suggest that AKT1 phosphorylates cGAS to suppress its enzymatic activity and results in downregulation of IFN β 1 production (Seo *et al.*, 2015). In contrast to the negative role of AKT1 on I-IFN production, our group has recently demonstrated that in response to viral infection, AKT3 expression is significantly enhanced in macrophages and promotes IFN β 1 induction (Xiao *et al.*, 2020). It is not fully understood whether and how AKT2 could affect I-IFN production.

In this study, we discovered that *Akt2* expression was downregulated in macrophages upon treatment with IFN β 1, the Toll-like receptor7/9 (TLR7/9) agonists, and during viral infection or during TMPD (N, N, N', N'-tetramethyl-p-phenylenediamine)-induced SLE. Disruption of *Akt2* enhanced the production of IFN β 1 and protected mice from viral infection. Conversely, *Akt2* deficiency led to the much worse SLE for increased IFN β 1 production. Mechanismly, AKT2 could directly bind and phosphorylate IRF3 at Thr207, which worked together with 14-3-3 ϵ to restrain the nuclear translocation of IRF3. In addition, AKT2 but not AKT2 kinase-dead mutant overexpression aggravated viral infection in zebrafish larvae, while overexpression of the IRF3-T207A promoted IFN β 1 production and reduced viral infection which was not reversed by AKT2 in zebrafish larvae. These data have demonstrated that AKT2 phosphorylates IRF3-T207 to reduce IRF3 nuclear localization and IFN β 1 induction, providing either protective or pathogenic role in SLE and viral infections.

Results

Akt2 expression is negatively correlated with IFN β 1 production

We firstly examined the distribution of AKT members in different organs. In contrast to the dominant expression of *Akt3* in brain, *Akt1* was widely expressed and *Akt2* was mainly expressed in heart, liver, and kidney (Fig EV1A). The expression levels of *Akt1* and *Akt2* were downregulated, while *Akt3* levels were upregulated in livers from vesicular stomatitis virus (VSV)-infected mice (Fig EV1B). We also confirmed the decreased *Akt2* expression in spleen and lung from VSV-infected mice (Fig EV1C), as well as from hepatitis B virus (HBV)-infected hepatocellular carcinoma (HCC) patients (Fig EV1D) that is consistent with the reduced AKT2 expression in livers from HBV-infected patients provided by the GEO database (Fig 1A, left panel). *Akt2* mRNA levels were also substantially downregulated in brain or lung from Japanese encephalitis virus (JEV)-infected or the influenza virus (H7N9, H1N1/PR8)-infected mice, respectively (Fig 1B). Moreover, the reduced *Akt2* mRNA expression was detected in bronchial epithelial cells upon H1N1 infection (Fig 1A, right panel), and in murine

peritoneal elucidated macrophages (PEMs) after treated with lipo-poly(I:C) to activate the RIG-1/MAVS pathway or treated with lipo-poly(A:T), lipo-ISD and HSV-1 to activate the cGAS/STING pathway (Fig 1C). Then, we also detected the decreased expression of total AKT2 and the phosphorylated AKT2-Ser474 at protein levels in VSV-infected PEMs (Fig EV1E).

Notably, we found that the mRNA levels of *Akt2* were negatively correlated with *Ifnb1* mRNA levels in VSV-infected PEMs, or in *Listeria monocytogenes* (LM) infected bone marrow-derived macrophages (BMDMs) (Fig 1D). Therefore, to investigate whether the IFN β 1/IFNAR signaling was responsible for *Akt2* expression, we obtained PEMs from the I-IFN receptor-deficient (*Ifnar1* KO) mice which hardly produced *Ifnb1* and *Cxcl10* in response to VSV infection or lipo-ISD treatment (Fig EV1F), ensuring PEMs from *Ifnar1* KO mice were defective in response to IFN β 1 stimulation. Interestingly, *Akt2* expressions were no longer downregulated in VSV-infected or lipo-ISD-treated PEMs from the *Ifnar1* KO mice (Fig 1E).

The IFN β 1/IFNAR signaling activates several key downstream effectors, and which one could participate in the suppression of *Akt2* expression? To answer this, WT PEMs were pretreated with various inhibitors targeting IFN β 1/IFNAR downstream proteins, including signal transducer and activator of transcriptions (STATs), p38, activator protein-1 (AP-1), nuclear transcription factor kappa-B (NF- κ B), and only the inhibitors targeting STAT3 and STAT6 (not STAT5) could prevent the downregulation of *Akt2* expression (Fig 1F). Furthermore, in the cytokine-activated Janus kinase (JAK)/STAT signaling cascade, the suppressors of cytokine signaling (SOCS) family members, especially SOCS1 and SOCS3, are induced by I-IFN stimulation, which then inhibit STAT activity to form a negative feedback loop (Morris *et al.*, 2018). Knockdown of *Socs1* or *Socs3* expression by siRNAs further reduced *Akt2* mRNA levels and enhanced I-IFN production after VSV treatment (Fig EV1G). Those results indicate that during viral infection, the IFN β 1/IFNAR signal decreases *Akt2* expression via STAT3/STAT6, and knockdown of SOCS1/SOCS3 could release their inhibition on STAT3/6 and further reduce *Akt2* expression.

To elucidate whether AKT2 regulated *Ifnb1* production, PEMs were treated with the AKT2 selective inhibitor CCT128930 (Fig 1G) or *Akt2* was knocked down by siRNA (Figs 1H and EV1H). After stimulated with lipo-poly(I:C), lipo-poly(A:T), lipo-ISD or infected with VSV and HSV-1, inhibition of AKT2 or knockdown of *Akt2* both enhanced the mRNA levels of *Ifnb1* in PEMs (Fig 1G and H). These data suggest that *Akt2* expression is reduced upon stimuli or viral infection, and *Akt2* negatively regulates IFN β 1 production.

AKT2 kinase activity is indispensable to attenuate I-IFN production in macrophages and in zebrafish larvae

To better understand the AKT2 function, we next used the *Akt2* knock-out (KO) mice. PEMs, BMDMs, and embryonic fibroblasts (primary-MEFs) were prepared from WT and *Akt2* KO mice. *Akt2* KO macrophages showed enhanced *Ifnb1* production after treated with various stimuli to activate the RIG-1/MAVS pathway or the cGAS/STING pathway (Figs 2A and EV2A). The ISGs including *Ifna4*, *Cxcl10*, and *Ccl5* were also induced at higher levels in *Akt2* KO PEMs upon VSV infection (Fig 2B). In addition, TLR3 and TLR4 pathway both can converge to induce *Ifnb1*, and *Akt2* KO PEMs also produced higher levels of *Ifnb1* upon treated with poly(I:C) to

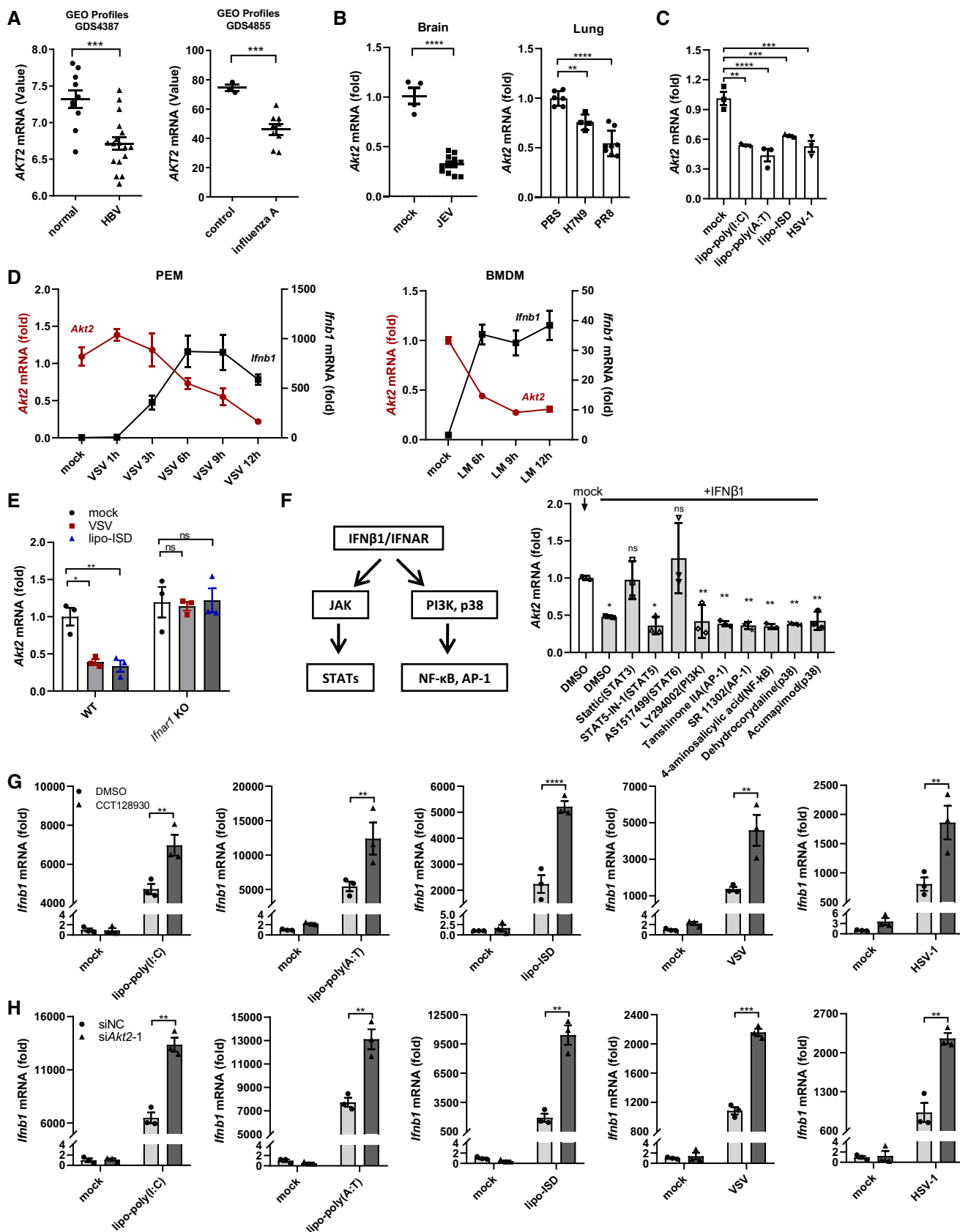


Figure 1.

Figure 1. Akt2 expression is negatively correlated with IFN β 1 production.

- A The mRNA value of *AKT2* was analyzed in the GEO Profiles from the liver explant of hepatitis B virus (HBV)-associated acute liver failure (ALF) patients (GDS4387/225471_s_at) and from bronchial epithelial cells with pandemic and seasonal H1N1 influenza virus infections *in vitro* (GDS4855/203808_at). normal, $n = 10$; HBV, $n = 17$; control, $n = 3$; influenza A, $n = 9$.
- B The mRNA expression of *Akt2* in the brain homogenates of WT mice with JEV injection (5.0×10^6 PFU/g, i.v.) or in the lung of WT mice with H7N9 ($10^{5.5}$ EID₅₀, i.n.) and PR8 infection (10 LD₅₀, i.n.) were detected by quantitative reverse transcription-PCR (qRT-PCR). Mock, $n = 4$; JEV, $n = 12$; PBS, $n = 6$; H7N9, $n = 4$; PR8, $n = 8$.
- C The qRT-PCR analysis of *Akt2* mRNA in PEMs stimulated with lipo-poly(I:C) (1 μ g/ml), lipo-poly(A:T) (1 μ g/ml), lipo-ISD (3 μ g/ml), or HSV-1 (MOI, 1) for 6 h. $n = 3$, respectively.
- D The mRNA of *Akt2* (red line) and *Ifnb1* (black line) were analyzed by qRT-PCR in the mock and VSV (MOI, 1) or LM (MOI, 1)-stimulated PEMs or BMDMs at the indicated time. Mock and VSV, $n = 4$; mock and LM, $n = 3$.
- E The mRNA levels of *Akt2* in WT ($n = 3$) and *Ifnar1* KO ($n = 3$) PEMs stimulated with VSV and lipo-ISD for 6 h were detected by qRT-PCR.
- F PEMs were pretreated with the indicated inhibitors for 2 h and stimulated with recombinant of IFN β 1 (1 μ g/ml) for another 3 h, followed by qRT-PCR for detection of the *Akt2* mRNA levels. DMSO, $n = 2$; inhibitors, $n = 3$.
- G, H PEMs were pretreated with DMSO or AKT2 inhibitor CCT128930 (10 μ M) (G) for 2 h, or knocked down of *Akt2* with si*Akt2*-1 (20 nM) for 48 h (H), then the mRNA level of *Ifnb1* was measured by qRT-PCR after lipo-poly(I:C), lipo-poly(A:T), lipo-ISD, VSV, or HSV-1 stimulation for another 6 h. $n = 3$, respectively.

Data information: * $P < 0.05$, ** $P < 0.01$, *** $P < 0.001$, **** $P < 0.0001$ and ns, not significant ($P > 0.05$); using unpaired *t*-test (A, B left panel), or one-way ANOVA test (B right panel, C and F), or two-way ANOVA test (E, G and H). Data are from two (F) or at least three independent biological replicates (C–E, G, H). Error bars (A and B, mean \pm SD; C–H, mean \pm SEM).

Source data are available online for this figure.

activate the TLR3 pathway or treated with LPS to activate the TLR4 pathway (Fig 2C). Following I-IFN production in *Akt2* KO macrophages, we further asked whether this affected bystander cells. WT or *Akt2* KO PEMs were stimulated with lipo-poly(I:C) for 3 h and washed several times to remove any residual lipo-poly(I:C). Fresh medium was added to WT or *Akt2* KO PEMs for another 9 h to collect cell medium, which was used to stimulate MEFs or PEMs. The culture medium from *Akt2* KO PEMs indeed induced higher *Ifnb1*, *Ifn4* production in MEFs or *Cxcl10*, *Ifit1*, *Mx1* production in PEMs (Fig EV2B). This suggests that *Akt2* KO macrophages not only enhance I-IFN production but also enhance the ISG expression in bystander cells such as PEMs and MEFs, therefore better preventing the viral infection and propagation. Consistent with *Akt2* KO PEMs (Fig 2A–C), *Akt2* KO primary-MEFs also enhanced *Ifnb1* mRNA level and reduced the amount of GFP-fused VSV infection shown by immunofluorescence microscopy or FACS assays (Figs 2D and EV2C). Moreover, after VSV infection, overexpression of AKT2 in MEFs and HEK293T cells restrained *Ifnb1* expression (Fig 2E), and IFN β 1-reporter luciferase assay confirmed that AKT2 inhibited IFN β 1 transcription in a dose-dependent manner (Fig EV2D).

Because AKT2 kinase activity is pivotal for its biological function in various cell types, we next overexpressed the kinase-dead mutant AKT2-T309A/S474A in HEK293T cells to explore whether AKT2 kinase activity was functioned in suppressing IFN β 1 production. When co-expressed with TBK1 or infected with VSV, AKT2 reduced the IFN β 1 luciferase readings, while the AKT2-T309A/S474A failed to inhibit this (Figs 2F and EV2E).

To verify the *in vivo* antiviral function of AKT2 or its kinase-dead mutant AKT2-T309A/S474A, we employed the zebrafish model as previously described (Meng *et al*, 2016; Guerra-Varela *et al*, 2018). Zebrafish can be generated in short term to express the interested proteins and is responsive to VSV infection. We used mpeg1-mCherry transgenic zebrafish larvae in which macrophage-lineage cells express mCherry and could be monitored *in vivo*. AKT2 mRNA was transcribed *in vitro* and injected into zebrafish embryos for 48 h to ensure AKT2 expression at protein levels (Fig EV2F), followed by VSV infection. We observed the colocalization of GFP-fused VSV (green) with mpeg1-mCherry macrophages (red) in the dorsal muscle, brain, and abdominal vessels of zebrafish larvae

(Figs 2G and EV2G, indicated by arrows). Zebrafish larvae overexpressing AKT2 reduced *ifn1* mRNA levels, displayed severer tissue damages in eye and trunk muscle, and decreased the survival rates (Fig 2H). In contrast, zebrafish larvae overexpressing the AKT2-T309A/S474A no longer aggravate viral infection than PBS control (Fig 2H). Together, we have demonstrated that AKT2 inhibits *Ifnb1* expression and this is dependent on AKT2 kinase activity.

AKT2 restrains IRF3 nuclear translocation via 14-3-3 ϵ

To gain mechanistic insight into the function of AKT2 on suppression of IFN β 1 production, we employed the IFN β 1 reporter luciferase system in HEK293T cells. Overexpression of AKT2 reduced MAVS-, TRIF-, or TBK1-induced IFN β 1 luciferase readings, but could not affect the constitutively active form IRF3-5D-mediated IFN β 1 transcription (Figs 3A and EV3A). When IRF3 or IRF3-5D was reconstituted into HEK293T-IRF3-KO cell line (Fig EV3B), AKT2 repressed IRF3 but not IRF3-5D-induced IFN β 1 luciferase activity in response to VSV infection (Fig 3B). Furthermore, when *Irf3* was knocked down by siRNAs (Fig EV3C), *Akt2* KO PEMs failed to further enhance *Ifnb1* levels under VSV infection (Fig 3C). These data indicate that AKT2 inhibits IFN β 1 production via IRF3.

AKT2 did not affect IRF3 transcription and translation (Fig EV3D, 3D-right panel). To explore whether AKT2 interacted with IRF3 endogenously, cell lysates of WT or *Akt2* KO PEMs were prepared for immunoprecipitation using anti-AKT2 antibody, followed by immunoblotting using anti-IRF3 antibody (Fig 3D, left panel). Alternatively, cell lysates were prepared for immunoprecipitation using anti-IRF3 antibody, followed by immunoblotting using anti-AKT2 antibody (Fig 3D, right panel). Both sets of data confirmed the endogenous association between AKT2 and IRF3. To map their interaction, HA-tagged AKT2 and Flag-tagged IRF3 or their truncations were co-expressed in HEK293T cells as indicated (Fig EV3E). Immunoprecipitation with anti-HA or anti-Flag antibodies was performed, which showed that the N terminus of AKT2 interacted with the IAD-domain of IRF3 (Fig EV3E). Next, GST-tagged AKT2 and His-tagged IRF3 were purified from *E. coli* to verify their direct interaction via the pull-down assay (Fig 3E). As a master transcription factor, IRF3 is phosphorylated and undergoes dimerization to

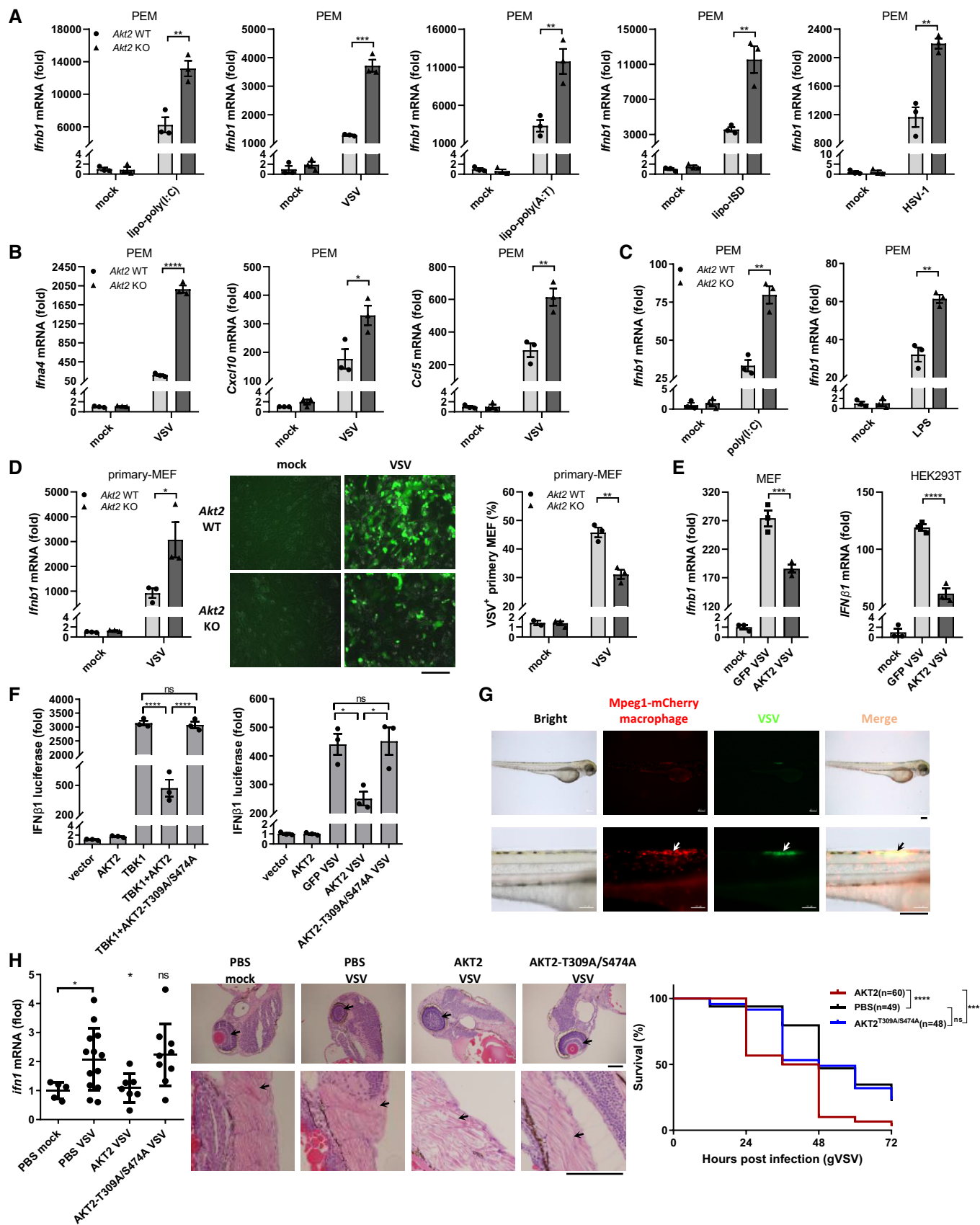


Figure 2.

Figure 2. AKT2 kinase activity is indispensable to attenuate I-IFN production in macrophages and in zebrafish larvae.

- A, B qRT-PCR detection for the mRNA expression of *Ifnb1* (A), *IfnA4*, *Cxcl10* and *Ccl5* (B) in WT ($n = 3$) and *Akt2* KO ($n = 3$) PEMs stimulated with lipo-poly(I:C), VSV, lipo-poly(A:T), lipo-ISD or HSV-1 for 6 h.
- C The expression of *Ifnb1* mRNA level by qRT-PCR in WT ($n = 3$) and *Akt2* KO ($n = 3$) PEMs treated with poly(I:C) (10 $\mu\text{g/ml}$) for 6 h (left panel) or LPS (1 $\mu\text{g/ml}$) for 2 h (right panel).
- D The expression of *Ifnb1* in WT ($n = 3$) and *Akt2* KO ($n = 3$) primary-MEFs with VSV treatment (MOI, 0.1) for 6 h was measured by qRT-PCR (left panel). After VSV treatment for 3 h, the culture suspension was discarded and washed 3 times with PBS, then primary-MEFs were cultured with fresh medium for another 15 h for analysis of the VSV-infected (GFP) primary-MEFs by fluorescence microscope (middle panel, representative images) and by FACS assay (right panel). Bar, 100 μm .
- E MEF (left panel, $n = 3$) and HEK293T cells (right panel, $n = 3$) were transfected with AKT2 for 24 h and stimulated with VSV for 6 h, then cells were harvested for the detection of mRNA expression of *Ifnb1* by qRT-PCR.
- F IFN β 1 luciferase assays of HEK293T cells with transfection of AKT2/AKT2-T309A/S474A and TBK1 ($n = 3$) or infection of VSV ($n = 3$). Protein expression levels are shown in Fig EV2E.
- G Zebrafish larva at 48 h after fertilization were micro-injected GFP-fused VSV (1×10^3 PFU/larvae) for 18 h, then the representative images of VSV-infected zebrafish larva were collected by fluorescence microscope. The infected area (GFP) and macrophages (Red) are indicated by arrows. Bars, 200 μm .
- H Zebrafish larvae were overexpressed the indicated protein for 48 h and challenged with VSV for another 6 h, then the mRNA levels of *ifn1* in zebrafish larvae were measured by qRT-PCR (left panel). Every dot represents three zebrafish embryos. Horizontal square bracket shows the statistical analysis of the comparison with "PBS mock", the rest shows the comparison with "PBS VSV". PBS mock, $n = 5$; PBS VSV, $n = 13$; AKT2 VSV, $n = 7$; AKT2-T309A/S474A VSV, $n = 9$. H&E staining (middle panel) and survival rates (Kaplan–Meier curve) (right panel) were collected from zebrafish larvae after VSV micro-injection for 18 h or longer. The arrows indicated the VSV-infected eye and skeletal muscle in zebrafish larvae. Bars, 100 μm .

Data information: * $P < 0.05$, ** $P < 0.01$, *** $P < 0.001$, **** $P < 0.0001$ and ns, not significant ($P > 0.05$); using a one-way ANOVA test (E, F, H left panel), or two-way ANOVA test (A–C, D left and right panel), or log-rank (Mantel–Cox) test (H right panel). Data are from three independent experiments (A–C, D left and right panel, E, F) or representative of three independent biological replicates (D middle panel, G, H). Error bars (A–F, mean \pm SEM; H, mean \pm SD).

Source data are available online for this figure.

translocate into the nuclei and induce *Ifnb1* transcription. Surprisingly, upon VSV infection or ISD treatment, *Akt2* deficiency did not affect IRF3 Ser396 phosphorylation and dimerization (Figs 3F and EV3F), but *Akt2* KO PEMs elevated the amount of IRF3 in the nuclei as measured by immunofluorescence (Figs 3G and EV3G) and immunoblotting (Fig 3H).

In previous reports, AKT2 can act as an anchor and cooperate with 14-3-3 to restrain the transcription-related factor p27^{Kip1} in cytoplasm (Fujita et al, 2002; Sekimoto et al, 2004). Based on the abundant expression of the 14-3-3 family members, that is, 14-3-3 ϵ (14-3-3epsilon, 14-3-3E) and 14-3-3 ζ (14-3-3zeta, 14-3-3Z) in macrophages (Munier et al, 2002), we performed IP and found that both 14-3-3 ϵ and 14-3-3 ζ interacted with AKT2 (Fig EV3H). We further explored whether 14-3-3 ϵ and 14-3-3 ζ might assist AKT2 to regulate the cellular location of IRF3 and expression of *Ifnb1*. Knockdown or overexpression of 14-3-3 ζ did not affect *Ifnb1* mRNA level or IFN β 1 luciferase activity (Fig EV3I). In contrast, knockdown of 14-3-3 ϵ could enhance *Ifnb1* production (Fig EV3J), implying that 14-3-3 ϵ , but not 14-3-3 ζ , might work together with AKT2 to inhibit *Ifnb1* transcription. Interestingly, 14-3-3 ϵ also interacted with IRF3 (Fig EV3K) and reduced the amount of IRF3 in the nuclei (Fig 3I), but did not affect IRF3-Ser396 phosphorylation and dimerization (Fig EV3L). In addition, co-expression of 14-3-3 ϵ with AKT2 further suppresses IFN β 1 in the IFN β 1 luciferase assays (Fig 3J), and knockdown of 14-3-3 ϵ enhanced the *Ifnb1* mRNA levels in WT PEMs, but this promotion was disappeared in *Akt2* KO PEMs (Fig 3K). These data together support that AKT2 directly binds IRF3, which cooperates with 14-3-3 ϵ , to prevent IRF3 translocation into the nuclei and suppress IFN β 1.

AKT2 phosphorylates IRF3 at Thr207 and blocks IRF3 activation

Our above findings indicated that inhibition of IFN β 1 expression was dependent on kinase activity of AKT2; therefore, we speculated that AKT2 kinase activity was critical to inhibit IRF3 translocation

into the nuclei. Next, Flag-tagged IRF3 was overexpressed in HEK293T-IRF3 KO cells together with HA-tagged AKT2 or the kinase-dead mutant AKT2-T309A/S474A. As expected, the AKT2 kinase-dead mutant failed to decrease the amount of IRF3 in the nuclei (Fig 4A). Using the Phos-tag gel, we detected the enhanced IRF3 phosphorylation levels in *Akt2* KO macrophages upon VSV challenge (Fig EV4A). To confirm that AKT2 regulated IRF3 phosphorylation in the *in vitro* kinase assay, HA-tagged AKT2 were enriched from HEK293T cells via immunoprecipitation and incubated with the purified His-tagged IRF3 protein from *E. Coli*. In the presence of AKT2, IRF3 was indeed phosphorylated that was shown as the shifted bands in the Phos-tag gel (Fig 4B, red arrow). To further identify the potential phosphorylation sites in IRF3, Flag-tagged IRF3 was overexpressed into HEK293T cells with AKT2 or the GFP control, next, anti-Flag immunoprecipitation was performed for the mass spectrometry (MS) analysis. Compared to the control, AKT2 overexpression induced IRF3 phosphorylations at Ser14, Ser173, S175, Thr180, Thr207 (Fig EV4B). We next mutated these residues into alanine (S14A, S173A/S175A, S180A, and T207A) to prevent phosphorylation. Only when the IRF3-T207A mutant was co-expressed, AKT2 no longer reduced the IFN β 1 luciferase activity (Figs 4C and EV4C). Moreover, the nuclear location and phosphorylation of IRF3-T207A were not changed by AKT2 (Fig 4D and E), and overexpression of IRF3-T207A did not change IRF3 Ser396-phosphorylation and dimerization after VSV stimulation (Fig EV4D). To verify the important function of IRF3-T207, IRF3-T207D (D, aspartic acid) was generated to mimic the phosphorylation status. Overexpression of IRF3-T207D inhibited IFN β 1 production, and AKT2 co-expression showed no further inhibition (Fig EV4E).

We were intrigued to assess the *in vivo* function of IRF3-T207A mutant, and then, zebrafish embryos were overexpressed with IRF3 or IRF3-T207A followed by VSV infection (Fig EV4F). Compared to the controls, zebrafish larvae expressing IRF3 enhanced the survival rates, and expressing IRF3-T207A displayed higher survival rates

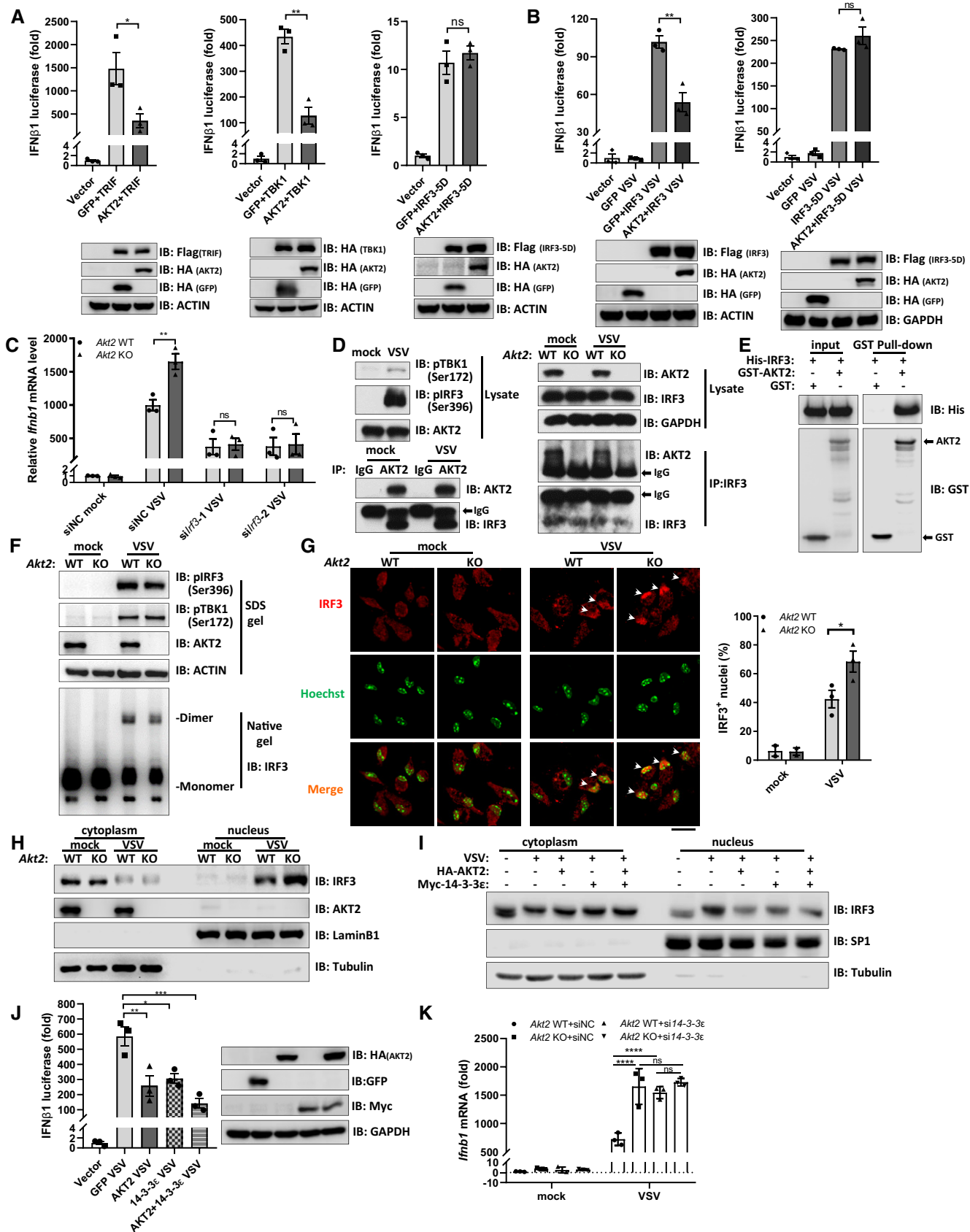


Figure 3.

Figure 3. AKT2 restrains IRF3 nuclear translocation via 14-3-3 ϵ .

- A, B IFN β 1 luciferase assays (upper panels) in HEK293T (A) and HEK293T-IRF3 KO (B) cells transfected with the indicated plasmids or infected with VSV. Immunoblot analysis showed the indicated constructs in HEK293T cells (bottom panels). $n = 3$, respectively.
- C The mRNA levels of *Irfn1* were measured by qRT-PCR in WT ($n = 3$) and *Akt2* KO ($n = 3$) PEMs with *Irf3* knockdown for 48 h and VSV treatment for 6 h.
- D WT and *Akt2* KO PEMs were infected with or without VSV for 6 h. Then, cell lysates of WT or *Akt2* KO PEMs were prepared for immunoprecipitation using anti-AKT2 antibody, followed by immunoblotting using anti-IRF3 antibody (left panel). Alternatively, cell lysates were prepared for immunoprecipitation using anti-IRF3 antibody, followed by immunoblotting using anti-AKT2 antibody (right panel) to detect the endogenous interaction between AKT2 and IRF3.
- E Immunoblot analysis of GST-AKT2 and His-IRF3 interaction in a GST pull-down assay.
- F Immunoassay of IRF3 in dimer or monomer form by native-gel and p-IRF3 (Ser396), p-TBK1 (Ser172), AKT2 and ACTIN by SDS-gel in WT and *Akt2* KO PEMs with VSV stimulation for 6 h.
- G Immunofluorescent microscopic imaging (left panel) and statistics analysis (right panel) for IRF3 nuclear translocation in WT and *Akt2* KO PEMs at 6 h post-VSV infection. IRF3 (red), Nuclei (Hoechst, green). The white arrows indicate the nuclei with IRF3 translocation. Mock, $n = 2$; VSV, $n = 3$. Bar, 20 μ m.
- H Immunoassay of IRF3, AKT2, LaminB1, and Tubulin in the nuclear and cytoplasmic fractions from the WT and *Akt2* KO PEMs after VSV treatment for 6 h. Tubulin and LaminB1 were used as cytoplasmic and nucleic protein loading control, respectively.
- I Immunoassay of IRF3, SP1, and Tubulin in the nuclear and cytoplasmic fractions of the HEK293T cells overexpressed with indicated constructs for 24 h and stimulated with VSV for 6 h. Tubulin and SP1 served as cytoplasmic and nucleic protein loading control, respectively.
- J IFN β 1 luciferase assays were performed in HEK293T cells transfected with AKT2 and 14-3-3 ϵ followed by VSV treatment. $n = 3$, respectively.
- K qRT-PCR analysis for the *Irfn1* mRNA levels in VSV-stimulated WT and *Akt2* KO PEMs with 14-3-3 ϵ siRNA pretreatment. $n = 3$, respectively.

Data information: * $P < 0.05$, ** $P < 0.01$, *** $P < 0.001$, **** $P < 0.0001$ and ns, not significant ($P > 0.05$); using a one-way ANOVA (A, B, J), or two-way ANOVA test (C, G right panel, K). Data are from three independent experiments (A–C, J and K), or representative of two or three independent biological replicates (D–I). Error bars (A–C, G, I and K, mean \pm SEM).

Source data are available online for this figure.

(Fig 4F, left panel) with less tissue damages (Fig 4F, right panel) and the reduced amount of VSV copies (Fig 4G and EV4G). Importantly, AKT2 overexpression could aggravate VSV copies and reduce the survival rates in zebrafish larvae expressing IRF3, but not expressing the IRF3-T207A mutant (Figs 4G and H, and EV4G). The kinase-dead mutant AKT2-T309A/S474A was included as the control, which showed less VSV copies in zebrafish larvae when compared to those expressing the WT AKT2 (Fig 4G). Collectively, these results have demonstrated that AKT2 depends on its kinase activity to phosphorylate IRF3 at Thr207 for preventing I-FN production and antiviral effects.

Targeting AKT2 enhances antiviral defense in mice

Akt2 KO mice showed normal percentages of macrophages (CD11b⁺F4/80⁺) in bone marrow (BM) and spleen, or normal macrophage development *ex vivo* derived from BM measured by FACS or quantitative reverse transcription-PCR (qRT-PCR) for the mRNA levels of adhesion G protein-coupled receptor E1 (*Adgre1*, also known as F4/80) and Mer tyrosine kinase (*MerTK*) (Fig 5A and Appendix Fig S1A). We have shown that *Akt2* KO PEMs enhanced IRF3 activity, and previous work suggests that the host could induce RIPA (RLR-induced IRF3-mediated pathway of apoptosis) to eliminate viral infection and pathogenesis (Chattopadhyay *et al*, 2016; Chattopadhyay & Sen, 2017). Therefore, we examined and found that in the absence or presence of viral infection, *Akt2* deficiency in PEMs did not obviously affect cell apoptosis (Appendix Fig S1B). This excludes the possibility that AKT2 might influence macrophage apoptosis to contribute to its antiviral function. *Akt2* KO mice also showed normal percentages of CD4⁺ T cells, CD8⁺ T cells, or B220⁺ B cells in thymus, spleen, or BM (Appendix Fig S1C). We next used VSV to infect WT and *Akt2* KO mice and evaluate the *in vivo* function of *Akt2* on antiviral defense. After VSV challenge, *Akt2* KO mice enhanced the survival rates (Fig 5B) and elevated *Irfn1* mRNA expression in livers, spleens, or lungs (Fig 5C) as well as serum IFN β 1 concentrations (Fig 5D). Moreover, the amount of VSV in

the liver of *Akt2* KO mice was reduced than that of WT mice (Fig 5E).

To verify the role of *Akt2*-deficient immune cells, we adoptively transferred WT and *Akt2* KO BMs respectively to reconstitute the irradiated CD45.1 recipient mice, followed by VSV challenge (Fig EV5A). The reconstituted CD45.1 *Akt2* KO mice showed higher survival rates with the increased concentrations of serum IFN β 1 (Fig 5F), which also reduced the copy numbers or titers of VSV from livers, spleens, or lungs (Fig 5G and H). To further explore the *in vivo* function of *Akt2*-deficient macrophages, we followed a previous study to effectively delete macrophages *in vivo* by clodronate liposome treatment (Jordan *et al*, 2003). Then, these mice were intravenous injected with WT and *Akt2* KO BMDMs followed by VSV challenge (as indicated in Fig EV5B). The mice reconstituted with *Akt2* KO-macrophages also enhanced serum IFN β 1 concentrations (Fig EV5C).

What's more, to ascertain if AKT2 might be a potential target to enhance antiviral effect in the host, the AKT2 selective inhibitor CCT128930 was used to treat mice, which indeed enhanced the survival rates in response to VSV infection (Fig 5I). These data together demonstrated that deletion or blocking AKT2 could be an effective strategy to enhance I-FN production and facilitate the host against viral infection.

Akt2 is associated with the pathology of SLE

Given that heightened I-FN is a prominently hallmark in SLE patients and correlated with disease severity (Bengtsson & Ronnblom, 2017), we next assessed how *Akt2* functioned in TMPD-induced murine SLE model. The expression of *Akt2* in different organs or tissue from TMPD-induced mice was analyzed at 2 weeks (the early stage) or 12 weeks (the late stage). *Akt2* expression was reduced in peritoneal infiltrating cells (PICs) at both the early and late stages, as well as in liver and lung at the late stage (Fig EV5D and E). Consistently, the expression of *Akt2* was decreased in the PEMs after treated with R848 or CpG to activate the TLR7 and TLR9

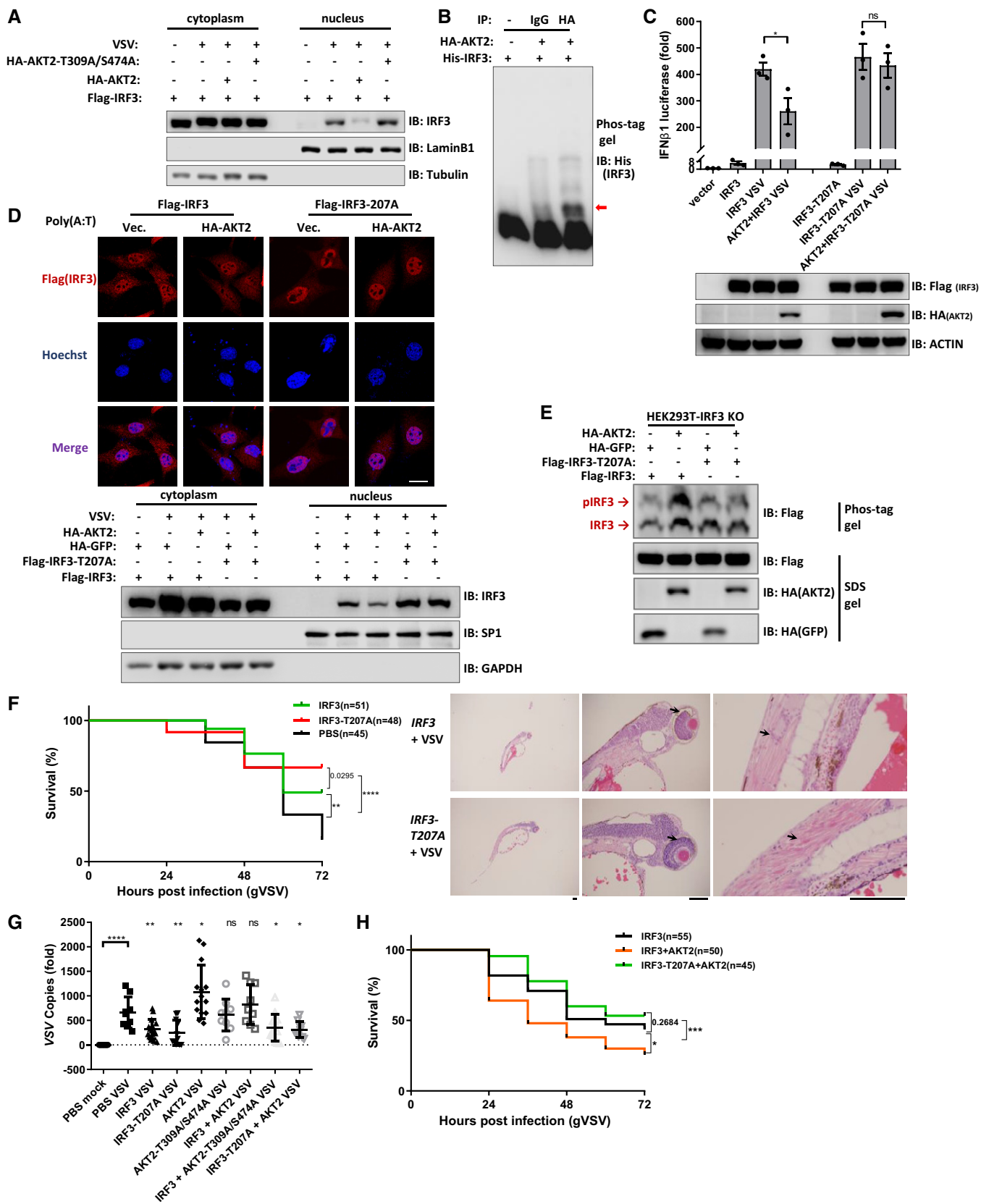


Figure 4.

Figure 4. AKT2 phosphorylates IRF3 at Thr207 and blocks IRF3 activation.

- A Immunoblot analysis of IRF3 in the cytoplasmic and nucleic fractions of HEK293T-*IRF3* KO cells with overexpression of IRF3 and AKT2 or AKT2-S309A/T474A.
- B Immunoblot analysis of *in vitro* kinase assay by the phosphorylation gel. HA-AKT2 was immunoprecipitated from HEK293T cells by anti-HA/IgG antibody and Protein-G beads, and His-IRF3 was purified from *E.coli* cells by anti-His antibody-conjugated agarose beads. His-IRF3 alone and anti-IgG-beads added with His-IRF3 served as controls. The red arrow indicated the phosphorylated IRF3.
- C IFN β 1 luciferase assays and immunoblot analysis showed the HEK293T-*IRF3* KO cells with overexpression of the indicated plasmids for 24 h and VSV infection for 6 h. $n = 3$, respectively.
- D Immunofluorescence microscopy (top panel) of AKT2-, Flag-IRF3-, or Flag-IRF3-T207A-overexpressed MEF cells after poly(A:T) stimulation for 6 h. Flag (IRF3, red) and Hoechst (nuclei, blue). Immunoassay of nuclear-cytoplasm extractions (bottom panel) from HEK293T-*IRF3* KO cells with overexpression of the indicated plasmids for 24 h followed by VSV infection for 6 h. GAPDH and SP1 were used as cytoplasmic and nucleic protein loading control, respectively. Bar, 20 μ m.
- E HEK293T-*IRF3* KO cells were overexpressed with indicated plasmids, and the cell lysates were conducted to immunoblot analysis by phosphorylation gel for the assay of phosphorylated IRF3 (the upper band) by anti-Flag antibody.
- F Survival rates (left panel) until 72 h and H&E staining (right panel) at 18 h of the zebrafish larvae with indicated protein expression and VSV challenge. The arrows indicated the VSV-infected eye and skeletal muscle in zebrafish larvae. Bars, 100 μ m.
- G qRT-PCR analysis of the VSV copies in overexpressed zebrafish embryos with the VSV challenge at 18 h later. Every dot represents three zebrafish embryos. Horizontal vertical square bracket shows the statistical analysis of comparison with "PBS mock", the rest shows the comparison with "PBS VSV". PBS mock, $n = 15$; PBS VSV, $n = 9$; IRF3 VSV, $n = 16$; IRF3-T207A VSV, $n = 11$; AKT2 VSV, $n = 14$; AKT2-T309A/S474A VSV, $n = 9$; IRF3 + AKT2 VSV, $n = 9$; IRF3 + AKT2-T309A/S474A VSV, $n = 13$; IRF3-T207A + AKT2 VSV, $n = 10$.
- H The survival rates of over-expressed zebrafish larvae as long as 72 h after the VSV challenge.
- Data information: * $P < 0.05$, ** $P < 0.01$, *** $P < 0.001$, **** $P < 0.0001$ and ns, not significant ($P > 0.05$); using a one-way ANOVA test (G), or two-way ANOVA test (C), or log-rank (Mantel-Cox) test (F left panel and H). Data are from at least three independent experiments (C), or representative of three independent experiments (A, B, D-H). Error bars (C, mean \pm SEM; G, mean \pm SD). Source data are available online for this figure.

pathways (Fig EV5F), and both pathways were previously demonstrated to aggravate SLE (Celhar *et al*, 2012).

According to others' studies, the diffuse pulmonary hemorrhage (DPH) can occur in some SLE patients with the increased mortality (Aguilera-Pickens & Abud-Mendoza, 2018). We found that TMPD-treated *Akt2* KO mice developed more serious DPH and increased leukocyte recruitment than that in WT mice at 2 weeks (Fig 6A, left panel). In parallel, *Akt2* KO mice exhibited splenomegaly and disrupted splenic architecture (Fig 6A, right panel) with the elevated percentages of CD11b⁺ cells (Fig EV5G). Not only the expression of *Ifnb1* and *Ifna4* increased in PIC and peripheral blood mononuclear cells (PBMCs) (Fig 6B) but also the amount of nuclear IRF3 enhanced in PICs (Fig 6C) from TMPD-induced *Akt2* KO mice.

Next, CD45.1 mice were also adoptively transferred with CD45.2 WT or *Akt2* KO BMs and treated with TMPD for 12 weeks to induce SLE (Fig EV5H). CD45.1 *Akt2* KO mice showed severer DPH and splenomegaly (Fig EV5I). TMPD injection could induce strong immune responses and the formation of lipogranuloma which is adhering to the mesothelial surface of mice (Reeves *et al*, 2009). Additionally, TMPD-induced SLE is accompanied with glomerulonephritis with the elevated anti-dsDNA IgG level in serum. In CD45.1 *Akt2* KO mice, we observed the exacerbated lipogranulomas (Fig 6D), glomerulonephritis, and the enhanced anti-IgG staining in kidney after TMPD treatment for 12 weeks (Fig 6E). In agreement with this, CD45.1 *Akt2* KO mice developed higher amount of anti-dsDNA IgG in serum (Fig 6F), increased *Ifnb1* and *Ifna4* expression in PICs (Fig 6G), and enhanced percentages of B220⁺ and CD19⁺MHCII⁺ cells in PBMCs (Fig 6H).

We then confirmed the reduced expression of *AKT2* in PBMCs isolated from SLE patients, when compared that from healthy donors (Fig 6I). Also, the expression of *AKT2* was negatively correlated with *I-IFN* in CD14⁺ monocytes from SLE patients (Fig 6J). Interestingly, in resting PBMCs from SLE patients, IRF3 was located in the cytoplasm and *AKT2* was expressed at a relative higher level, which was contrast to the decreased *AKT2* expression and the increased amount of IRF3 in the nucleus once PBMCs were at

activated state (Fig 6K). Together, we demonstrated that *AKT2* plays a protective role in the pathology of SLE.

Discussion

Phosphorylation, dimerization, and nuclear accumulation are three hallmarks of IRF3 activation. A great number of studies have elucidated the mechanism of IRF3 phosphorylation, but less about how to regulate IRF3 translocation from cytoplasm to nuclei. Our study has provided a new perspective that cooperating together with 14-3-3 ϵ , *AKT2* binds and phosphorylates IRF3 at Thr207 to restrain IRF3 nuclear translocation and blunt IFN β 1 production. Once macrophage responds to viral infection, IFN β 1 is induced to downregulate *Akt2* expression, which leads to IRF3 release from the cytoplasm for its nuclear entry and the induction of I-IFN (Appendix Fig S3). Upon viral infection, TBK1 phosphorylates MAVS, TRIF, and STING to recruit IRF3, which then allows TBK1 to phosphorylate IRF3. Once phosphorylated, IRF3 is licensed to dissociate from them, dimerizes and entries into the nuclei. Since IRF3-Thr207 has no impact on IRF3 dimerization, we could speculate that like WT IRF3, IRF3-Thr207 is recruited to and then dissociated from the other adaptor proteins (STING/TRIF/TBK1). In addition, the luciferase reporter assays in Fig 3A and B have shown that IRF3-5D-induced IFN β 1 production was not affected by *AKT2* overexpression. This suggests that IRF3-5D might form a dimer and is not accessible to be phosphorylated by *AKT2* at Thr207. Previous work has suggested that PTEN antagonizes the PI(3)K/AKT pathway (Maehama & Dixon, 1998; Stambolic *et al*, 1998), and PTEN can positively facilitate IRF3 nuclear localization through de-phosphorylating IRF3 at Ser97 (Li *et al*, 2016). Those clues imply a possibility about whether PTEN could inactivate *AKT2*, which results in the reduced phosphorylation levels of IRF3 at Thr207 and allows IRF3 activation and I-IFN production.

Besides phosphorylation, other types of post-translational modifications (PTMs) are also critical for IRF3 activation, including

ubiquitination, methylation, acetylation, SUMOylation, and ADP-ribosylation. Further studies suggest that one type of PTMs might be related to other types of PTMs to affect IRF3 activation. For example, the prolyl isomerase Pin1 phosphorylates IRF3 at Ser339/Pro340, leading to IRF3 polyubiquitination and then degradation

(Saitoh *et al*, 2006); lysine methyltransferase nuclear receptor-binding SET domain 3 (NSD3) is associated with IRF3 directly and methylates IRF3 at K366, which can maintain IRF3 phosphorylation to promote I-IFN production (Wang *et al*, 2017). These studies suggest that different signal pathways are participated and

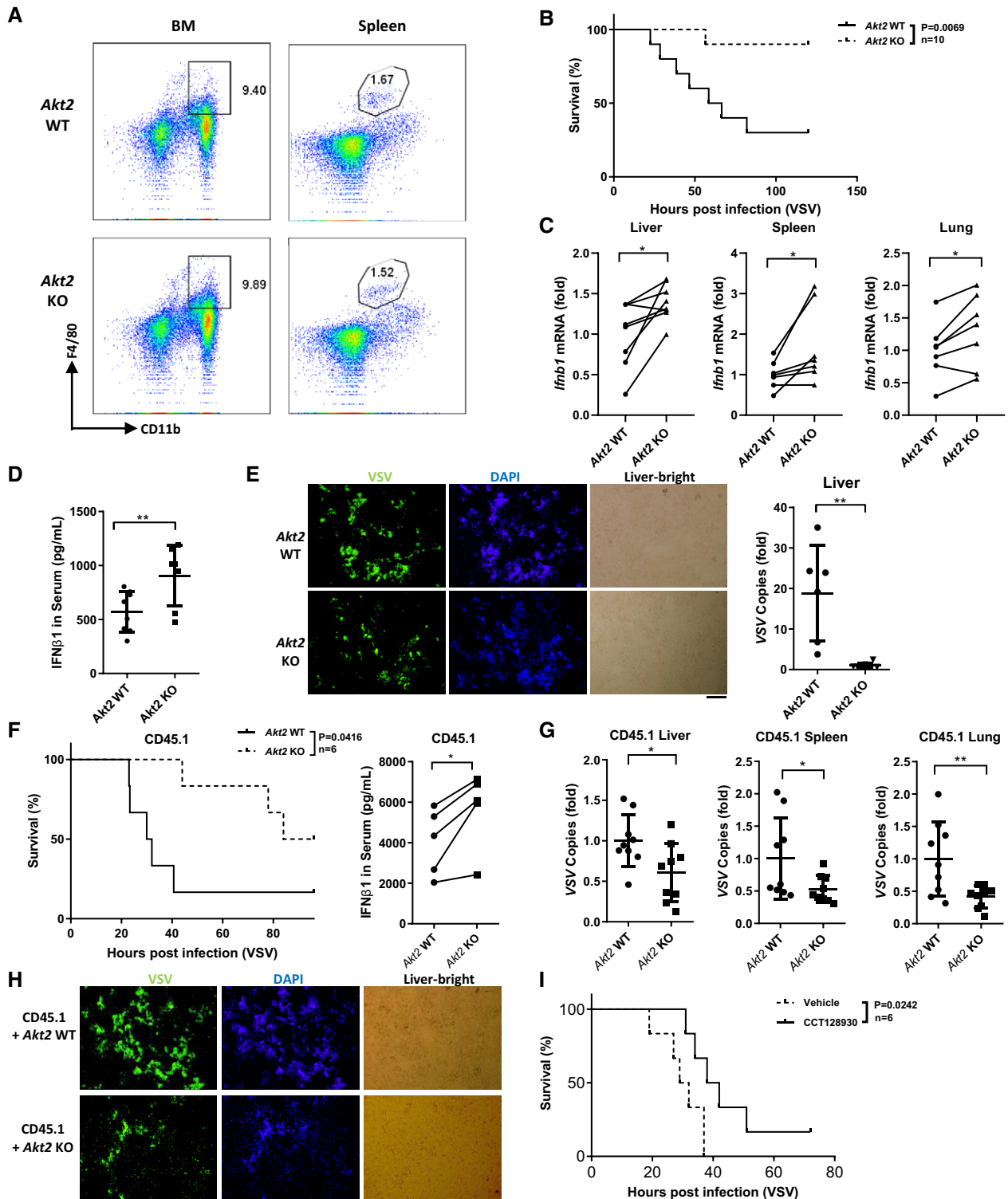


Figure 5.

Figure 5. Targeting AKT2 enhances antiviral defense in mice.

- A FACS analysis of the percentage of macrophages (CD11b⁺ F4/80⁺ cells) in WT and *Akt2* KO BM and spleen.
- B Survival rates of WT and *Akt2* KO mice after lethal dose injection of VSV during 120 h (1×10^7 PFU/g, i.v.).
- C qRT-PCR analysis of the *Ifnb1* mRNA expression in the liver ($n = 8$), spleen ($n = 7$) and lung ($n = 7$) of WT or *Akt2* KO mice 6 h after the injection of VSV (1×10^6 PFU/g, i.v.).
- D IFN β 1 concentrations from WT ($n = 8$) and *Akt2* KO ($n = 7$) serum were detected by ELISA 3 h after VSV infection (1×10^6 PFU/g, i.v.).
- E WT and *Akt2* KO mice were injected with VSV for 24 h (1×10^6 PFU/g, i.v.). Representative images of the VSV-infected cells (GFP) were collected by fluorescence microscope (left panel) and the VSV copies (WT, $n = 6$; *Akt2* KO $n = 7$) were measured by qRT-PCR (right panel) in the liver of mice. Bar, 100 μ m.
- F–H Bone marrow cells from WT and *Akt2* KO mice (CD45.2) were adoptively transferred to lethally irradiated CD45.1 mice and infected with VSV. Survival rates (F left panel), serum IFN β 1 concentrations (F right panel, $n = 5$), VSV copies (G, $n = 9$) and representative images (H) were analyzed as Fig 5B, D and E, respectively. Bar, 100 μ m.
- I Survival rates of WT mice that were intraperitoneal injected with CCT128930 (20 mg/kg) twice every other day before VSV infection (1×10^7 PFU/g, i.v.).

Data information: * $P < 0.05$, ** $P < 0.01$; using a paired t-test (C and F right panel), or unpaired t-test (D, E right panel and G) or log-rank (Mantel–Cox) test (B, F left panel and I). Data are representative of three independent experiments, respectively (A–I), in which the different groups of mice were sacrificed and quantified for indicated experimental purposes (C–E, F right panel, G). Error bars (D, E right panel and G, mean \pm SD).

Source data are available online for this figure.

cooperated to precisely regulate IRF3 activation. It is interesting to further reveal whether AKT2-mediated IRF3-Thr207 phosphorylation could affect or to be affected by other types of PTMs.

Antiviral responses are complicated processes including the early and late stages. We confirmed that *Akt2* deficiency could enhance *Ifnb1* and ISGs production at the early stage (Fig 2A and B), which could also affect bystander cells for the induction of ISGs (Fig EV2B). In addition, vRNA extracted from VSV was used to treat *Akt2* KO macrophages to mimic 5'pppRNA stimulation (Goulet *et al*, 2013), which differentially regulated the expression of several genes at the early or late stages. For example, *Akt2* KO PEMs enhanced the mRNA levels of *Ifnb1* and *Iffa4* at the early stage, but this enhancement was diminished at the late stage; in contrast, the mRNA levels of *Ccl2* and *Ccl5* were enhanced in *Akt2* KO PEMs at the late stage (Appendix Fig S2A). These results suggest that AKT2 might affect the expression of multiple genes directly or indirectly during different phases of antiviral responses. For instance, IRF7 is another IRF family member which could also induce *Ifnb1* transcription (Levy *et al*, 2002; Ning *et al*, 2011). We found that *Iffa* was enhanced in livers and lungs of *Akt2* KO mice (Appendix Fig S2B), and *Iffa* transcription is driven mainly by IRF7. IRF7 is also downstream of the IFN β 1/IFNAR pathway; therefore, *Iffa* enhancement might be indirectly induced by the increased IFN β 1 in *Akt2* KO macrophages. Future studies are needed to explore additional functions of AKT2, including its role in regulating IRF7 activation. In addition, AKT2 activation could induce glucose transporter 1 expression, glucose uptake, and lactate production in neoplastic cells (Moro *et al*, 2009). Interestingly, lactate was reported to inhibit RLR-mediated IFN production (Zhang *et al*, 2019). It is therefore worthy to test whether AKT2 might also affect lactate production to inhibit IFN production.

Meanwhile, the significance of AKTs has been studied extensively since its first discovery 30 years ago (Coffer & Woodgett, 1991). AKTs play critical roles in gene transcription, protein synthesis, proliferation, migration, autophagy, anti-apoptosis, and the maintenance of metabolic homeostasis (Dummler & Hemmings, 2007; Xue *et al*, 2015). AKTs also regulate immune cell development and immune responses (Zhang *et al*, 2013; Xue *et al*, 2015). We have noticed that in viral-infected macrophages, *Akt3* expression is upregulated as an ISG (Hubel *et al*, 2019; Xiao *et al*, 2020), while *Akt2* transcription is suppressed, which are both dependent on the

IFN β 1/IFNAR pathway. STAT is the key transcription factor to induce ISGs, and STAT3 has been identified to bind to *Akt2* promoter in website forecast (QIAGEN) or through ChIP experiment in HCC cells (Xie *et al*, 2018). In this study, we demonstrated that inhibition of STAT3/STAT6 could prevent the reduced *Akt2* transcription in Fig 1F; knockdown of *Socs1/Socs3*, which are key molecules in the negative feedback loop of the IFN β 1/IFNAR-JAK/STAT pathway, could release STAT3/STAT6 to further decrease *Akt2* expression in Fig EV1G. Importantly, our study elucidated that the downregulated expression of *Akt2* in macrophages might be used as a biomarker in I-IFN-related diseases including SLE. Apart from infections, I-IFN is positively related to the development of SLE, and the JAK/STAT pathway participates in the pathogenesis of SLE (Goropevsek *et al*, 2019). Therefore, targeting JAK/STAT is a promising strategy to protect SLE patients. Our study provides different perspectives about the underline mechanism: targeting JAK/STAT could not only block I-IFN signaling, but also maintaining *Akt2* expression in macrophages that could reduce IRF3 nuclei entry and inhibit I-IFN production. On the other hand, AKT2 is a critical negative regulator for I-IFN production, we propose a new application of the selective AKT2 inhibitor CCT128930 in antiviral therapy. Together, considering AKT2 expression and function, AKT2 could be used as a biomarker for diagnosis or a drug target in SLE or viral infection.

AKTs also play critical roles in the induction and progression of various tumors, and CCT128930 was previously investigated as an antitumor drug in preclinical studies (Yap *et al*, 2011). Tumor-associated macrophages (TAMs) are essential to promote tumor development, but I-IFN was previously reported to enhance tumor cell apoptosis (Parker *et al*, 2016). Interestingly, we found that when macrophages were treated with the genomic DNA from the tumor cell line MC38 and B16, *Akt2* was downregulated and negatively related to *Ifnb1* expression (Appendix Fig S2C). Moreover, *Akt2* was downregulated when macrophages are treated with IL-6 and TNF- α (Appendix Fig S2D), which are critical pro-inflammatory cytokines in the tumor microenvironments (TME). Could *Akt2* deficiency in TAMs enhance I-IFN production, which is able to shape TAM function to inhibit tumor development? In addition, several studies have indicated that AKT2, but not AKT1, could promote macrophage migration and phagocytosis (Shiratsuchi & Basson, 2007; Zhang *et al*, 2009), and TAM-mediated phagocytosis

facilitate tumor growth (Kitamura *et al*, 2015; Roy *et al*, 2018). Therefore, it is exciting to explore whether targeting AKT2 represents “one stone kills two birds” strategy, which not only reduces

tumor cell survival but also reverses the function of TAMs to better block tumor development. This potential application should be investigated using the *in vivo* tumor models in the future.

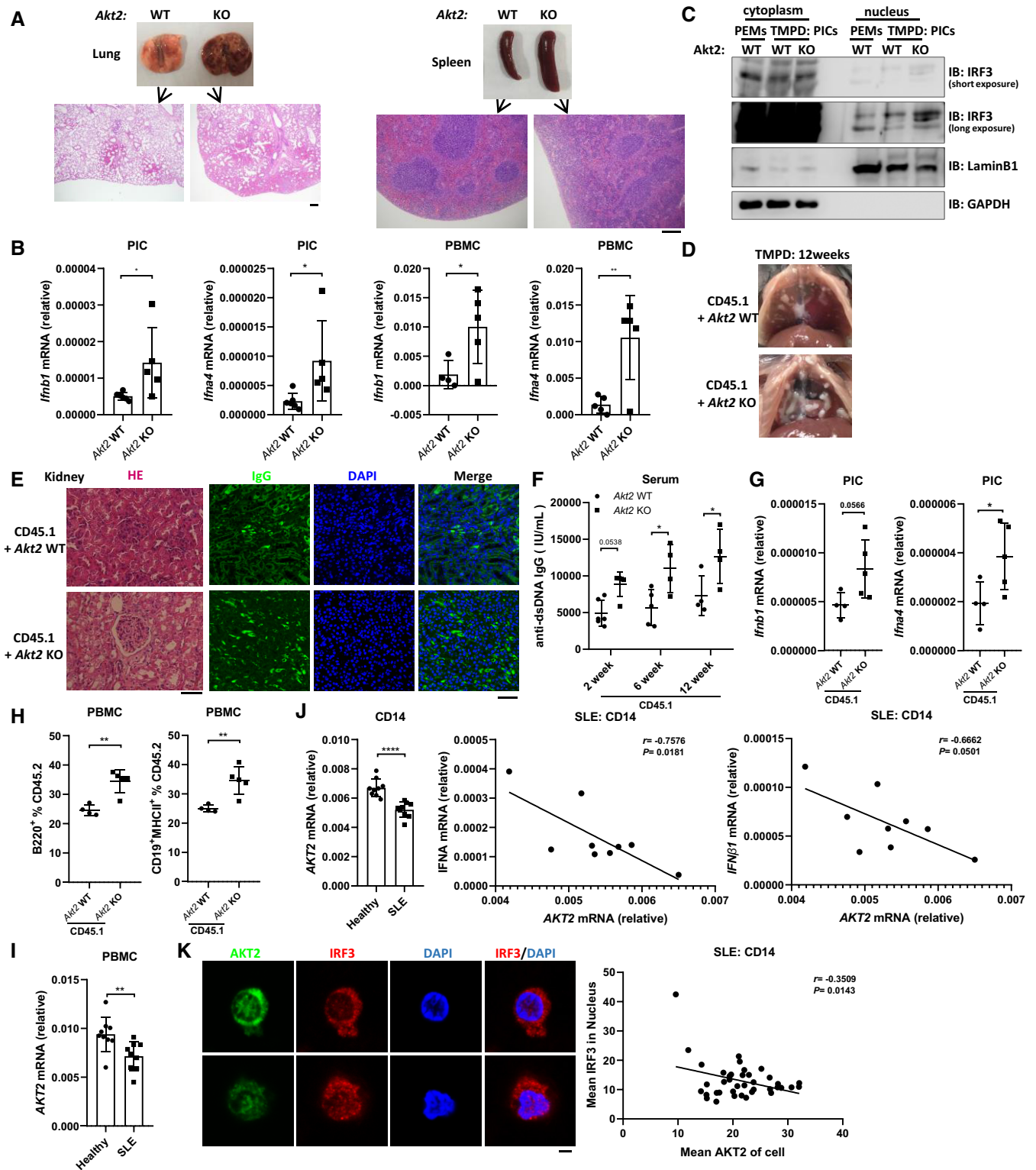


Figure 6.

Figure 6. Akt2 is associated with the pathology of SLE.

- A Representative images of lungs and spleens from WT and Akt2 KO mice treated with TMPD (500 μ l per mouse) for 2 weeks, and the corresponding H&E staining of the tissues. Bar, 200 μ m.
- B, C qRT-PCR analysis of the relative *Irfn1* and *Irfn4* mRNA expression levels in PICs ($n \geq 5$) and PBMCs ($n \geq 4$) (B), and immunoblot analysis of IRF3, LaminB1, and GAPDH in the PIC nuclear and cytoplasmic fractions (C) from WT and Akt2 KO mice treated with TMPD for 2 weeks. GAPDH and LaminB1 were used as cytoplasmic and nucleic protein loading control, respectively.
- D, E Representative images of lipogranulomas in peritoneal cavity (D), H&E staining (E left panel) and immunofluorescence of IgG deposits (E right panel) in the kidney sections were collected from WT and Akt2 KO bone marrow-reconstituted CD45.1 mice 12 weeks after TMPD treatment. Bar, 50 μ m.
- F–H Quantitative analysis of serum anti-dsDNA IgG antibody by ELISA (F, $n \geq 4$), mRNA expression levels of *Irfn1* and *Irfn4* in PIC by qRT-PCR (G, $n \geq 4$) and FACS analysis of the percentages of B220⁺ and CD19⁺MHCII⁺ cells in PBMC (H, $n \geq 4$) from WT and Akt2 KO bone marrow-reconstituted CD45.1 mice 12 weeks after TMPD treatment.
- I qRT-PCR analysis of the relative mRNA expression levels of AKT2 in PBMC isolated from SLE patients ($n = 9$) or healthy donors ($n = 9$).
- J qRT-PCR analysis of the relative mRNA expression levels of AKT2 (left panel) and *IFNA* (middle panel) or *IFN β 1* (right panel) in CD14-positive monocytes isolated from SLE patients ($n = 9$) or healthy donors ($n = 9$).
- K Immunofluorescence of IRF3 (Red), AKT2 (Green), DAPI (Blue, nucleus) in CD14⁺ cells from SLE patients followed by analysis of the cells about mean amount of AKT2 in this cell as well as mean amount of IRF3 in the same nucleus with ImageJ software. Cells ($n = 39$) were collected from 3 patients. Bar, 2 μ m.

Data information: * $P < 0.05$, ** $P < 0.01$, and **** $P < 0.0001$; using unpaired t-test (B, G–I, J left panel), or two-way ANOVA test (F), or correlation analyses (J middle and right panels, K right panel). Data are pooled from different individuals (I, J, K right panel) or representative of three independent experiments (A–H, K left panel). Error bars (B, F–J, mean \pm SD).

Source data are available online for this figure.

Materials and Methods

Mice

We thank Dr. Zhongzhou Yang for providing Akt2 KO mice and Dr. Qibin Leng and Dr. Jin Zhong for providing *Irfn1* KO mice. Age (8–24 weeks old)- and sex-matched mice were used for the *in vivo* and *in vitro* experiments. Mice were bred and maintained with approval by the animal facility of Shanghai Institute of Biochemistry and Cell Biology (protocol IBCB0057) under specific pathogen-free (SPF) conditions. All animal studies were approved by the Institutional Animal Care and Use Committee (IACUC) of the Institute of Biochemistry and Cell Biology, Center for Excellence in Molecular Cell Science, Chinese Academy of Sciences.

Human sample

This study was approved by the ethics committee of Ren Ji Hospital, Shanghai Jiao Tong University School of Medicine, Shanghai, China. All samples were collected with signed informed consent. According to the instructions, PBMCs were isolated by Lymphocyte Separation Medium 1.077 (YEASEN, #40503ES60), and CD14-positive cells were further selected from PBMCs (STEAMCELL, #17818).

Reagents, antibodies, and constructs

These reagents or kits were purchased from the indicated manufacturers: Poly(A:T) and LPS from Sigma; Poly(I:C), R848, CpG (ODN1668) from InvivoGen; CCT128930 from Selleck; M-CSF, IL-6, TNF- α , and IFN β 1 from PeproTech; Nuclear and cytoplasmic extracts kit (#P0027) from Beyotime; Clodronate liposome from FormuMa. Antibodies including p-AKT2 (Ser474, Cell Signaling Technologies, #8599S), AKT2 (Cell Signaling Technologies, #3063S), p-TBK1 (Ser172, Cell Signaling Technologies, #5483S), TBK1 (Cell Signaling Technologies, #3504S), p-IRF3 (Ser396, Cell Signaling Technologies, #4947S), AKT1 (Cell Signaling Technologies, #2938S), AKT3 (Cell Signaling Technologies, #14982), HRP-

ACTIN (Abcam, ab82226), HA (Cell Signaling Technologies, #3724S), rabbit control IgG (Abcam, ab172730), IRF3 (Santa Cruz Biotechnology, sc-9082 and Proteintech, 11312-1-AP), HRP-GAPDH (Proteintech, HRP-60004), GST (Proteintech, 10000-0-AP), His (Proteintech, 66005-1-Ig), LaminB1 (Proteintech, 12987-1-AP), Myc (Cell Signaling Technologies, #2276S), 14-3-3 ζ (Proteintech, 14881-1-AP), 14-3-3 ϵ (Proteintech, 11648-2-AP), SP1 (Proteintech, 21962-1-AP), Annexin V (Invitrogen, BMS306APC/100), 7AAD (BD, 559925) were purchased from the indicated manufacturers. CD11b-FITC (11-0112-82), F4/80-APC-Cy7 (123118), CD4-FITC (11-0041-81), CD8-APC (17-0081), B220-PE (12-0452), CD45.2-APC (17-0454-81), CD45.1-PerCP-Cy5.5 (45-0453-82) were purchased from Thermo (eBioscience). pCDNA3.1-HA-AKT2 was kindly provided by Daming Gao (SIBCB, CAS). pCDNA3.1-Flag-TRIF/TBK1/IRF3/IRF3-5D, pGL3-IFN β 1 luciferase reporter, pRL-TK-Renilla were kindly provided by Bing Sun (SIBCB, CAS). pcDNA3.0-HA-MAVS was kindly provided by Fajian Hou (SIBCB, CAS). The related mutations in AKT2 or in IRF3 were constructed by standard PCR cloning strategy. To purify proteins from *E. coli*, AKT2 was inserted into the pGEX4T-1-GST plasmid (GE Healthcare) with GST-tag in the N terminus and IRF3 was inserted into the pET-28a-His plasmid with 6xHis tag in the N terminus. Human 14-3-3 ζ and 14-3-3 ϵ cDNAs were amplified from reverse-transcribed cDNA of HEK293T cells. vRNA was prepared from VSV in Trizol (Takara).

Macrophage preparation and treatment

BMDMs were generated from BM cells followed by culturing in complete 1640 supplemented with 10% (vol/vol) FBS, penicillin and streptomycin (100 U/ml), and M-CSF (20 ng/ml) for 5–7 days. PEMs were harvested from mice injected peritoneally with 2 ml 3% Brewer thioglycolate medium for 4 days and cultured with complete DMEM supplemented with 10% (vol/vol) FBS and penicillin and streptomycin (100 U/ml). Primary MEFs were trypsin digested from mouse embryo at day13.5 without the fetal liver, expanded and cultured with complete DMEM. To active different pathways in macrophages, poly(I:C), poly(A:T), ISD, or vRNA were transfected via Lipofectamine 2000 (Invitrogen); or poly(I:C), LPS, VSV, or

HSV-1 were added in the culture medium. Genomic DNA from MC38 cells or B16 cells was transfected into PEMs via Lipofectamine 2000.

Animal experiment

8-week-old mice were infected with VSV intravenously (i.v.) at a dose of 10^7 pfu per gram of animal weight to monitor the survival rate. The inhibitor CCT128930 at a dose of 20 mg/kg or the DMSO control was injected intraperitoneally (i.p) twice every other day before VSV infection. Mice were infected with GFP-fused VSV at a dose of 10^6 pfu/g of animal weight and sacrificed at 3 h, 6 h, or 18 h to collect serum and organs. Serum was used to detect IFN β 1 concentrations by enzyme-linked immunosorbent assay (ELISA, PBL, #42400), and organs were collected for hematoxylin and eosin (H&E) staining or for RNA extraction followed by qRT-PCR assay. For adoptive transfer, BM cells were isolated from mice without erythrolysis and i.v. injected into the lethally irradiated CD45.1 recipient mice (2 million per mice). Alternatively, clodronate liposome (200 μ l/20 g) was i.v. injected twice every other day to delete endogenous macrophages, followed by i.v. transferring of BMDMs (3 million per mice), and mice were then infected with VSV.

SLE was induced by i.p. injection with 500 μ l of TMPD (Sigma, P2870) per mouse (female, 6–8 weeks old), and PBS was used as the control. 2 or 12 weeks after injection, mice were sacrificed for FACS assay or for the detection of serum anti-dsDNA IgG levels (kexinbiotech) by ELISA and others.

Overexpression and VSV challenge of zebrafish larvae

Ectopic overexpression and VSV challenge of zebrafish larvae were performed as previously described (Meng *et al*, 2016). Briefly, wild-type or mpeg:mCherry embryos were injected with the 50 pg (< 2 nl/embryo) of the *in vitro* transcribed mRNA (Thermo Fisher Scientific) in the first 20 min after fertilization. After 48 h, VSV was micro-injected (< 4 nl/larva) into the embryo yolk. After 6 or 18 h, zebrafish larvae were harvested to extract mRNA or for the microscopy assay.

FACS assay and microscopy assay

FACS assay and immunofluorescence assay were performed as described (Liu *et al*, 2020). Single cell suspension from spleen, BM, thymus, PEMs, and blood were prepared for immunostaining with anti-IRF3, anti-Flag, anti-AKT2, and other appropriate antibodies. Annexin V/7AAD staining or DAPI/Hoechst staining of PEMs was conducted according to the instruction. Data and images were collected with BD Accuri C6 and Fortessa, or Olympus BX51, Zeiss LSM880 Leica SP8 WLL, then analyzed with the respective software.

Cell culture and transfection

HEK293T and HEK293T-*IRF3* KO cells were kindly provided by FJ. Hou (SIBCB, CAS) transfected with plasmids using PEI (CAT#23966-2) (3.0 μ l for 1 μ g plasmid). Plasmids expressing target genes were induced into MEFs through Lipofectamine 3000 (Invitrogen). HEK293T cells and MEFs were cultured in complete DMEM. The empty or GFP plasmid was used as the control to keep the same

amount of total DNA. The pMIGR-IRES-GFP and pCL-10A plasmids were transfected into HEK293T cells and the retroviral supernatants were collected after 48 h to infect MEFs. GFP-positive cells were sorted to obtain the stable MEFs expressing the interested genes. siRNAs (20 nmol/ml) targeting *Akt2*, *SOCS1*, *SOCS3*, *14-3-3 ϵ* , *14-3-3 ζ* , and *Irf3* (GeneParma) were transfected into PEMs (0.3 million cells/well, 24-well plate) via Lipofectamine RNAiMAX (Invitrogen) for 48–72 h. The siRNA sequences are listed in Table EV1.

IFN β 1 Luciferase reporter assay

The plasmids expressing the indicated proteins (0.25 μ g), the IFN β 1 luciferase reporter (0.25 μ g), and the internal control TK-renilla (0.01 μ g) were transfected with 1.53 μ l PEI into HEK293T cells, which were 80–90% confluent in a 24-well plate. After 6–8 h, fresh culture medium was changed to culture the cells for at least another 18 h. If necessary, HEK293T cells were infected with or without VSV for 6 h. Then, cells were harvested to measure the luciferase readings with the guidance of a dual-luciferase assay kit (Promega, #0000456500). Briefly, culture supernatant was discarded, and cells were washed with PBS. Passive Lysis Buffer (diluted with water to 1 \times , 100 μ l/well) was added to lyse cells, and supernatants were collected. Next, 20 μ l lytic supernatants of each well were mixed with 20 μ l Luciferase Assay Buffer II and measured as Results 1. Then, 20 μ l Stop & Glo[®] Buffer was added for Results 2. Finally, we divided Result 1 by Result 2 to get the relative IFN β 1 Luciferase activity, and calculated the fold changes of IFN β 1 Luciferase activity by compared to the control groups.

Each experiment was performed in triple wells using the same plasmids synchronously for technical replicate; and three independent experiments were repeated. The data were shown from three independent experiments or from a representative experiment as indicated.

Immunoprecipitation, immunoblot, native PAGE

Immunoprecipitation and Mass-spec assay were performed as described previously (Xue *et al*, 2016; Xiao *et al*, 2020). In native PAGE, cells were collected in PBS without residuary FBS and lysed with cold lysis buffer. 8% acrylamide gel without SDS was pre-run at 40 mA for 30 min on ice, with 25 mM Tris-HCl (pH 8.4) in a cathode added 0.5% deoxycholate, and 192 mM glycine in anode chamber. Before immunoblotting, the cell lysates in the native loading buffer (Beyotime) were loaded on the gel and electrophoresed for 60 min at 200V on ice.

GST pull-down and the *in vitro* kinase assay

pGEX-4T-1-GST-hAKT2 and pET-28a-6*His-hIRF3 were transformed into *Escherichia coli* BL21 (DE3) (TranGen Biotech). Protein expression was induced via 0.25 mM IPTG treatment for 24 h at 16 $^{\circ}$ C. Recombinant proteins were harvested as described previously (Lu *et al*, 2019). The purified proteins at the same molar quantity including 6*His-hIRF3 and GST-hAKT2 or GST were incubated for 2 h followed by incubation with GST-beads for another 1 h at 4 $^{\circ}$ C in 400 μ l pull-down buffer (20 mM Tris-HCl, 100 mM NaCl, 5 mM MgCl₂, 1 mM EDTA, 1 mM DTT, 0.5% (v/v) NP-40 and 10 mg/ml BSA, pH 7.5), and washed four times with the same buffer. Samples

were treated with the addition of SDS loading buffer and the supernatants were subjected to 10% SDS-PAGE.

To ensure AKT2 kinase activity, HA-AKT2 was immunoprecipitated from HEK293T cells using anti-HA antibody, and anti-IgG antibody was used as a control. Samples were then incubated with 6*His-hIRF3 at 30°C for 30 min with gentle shaking in the kinase reaction buffer (Cell Signaling Technology). This kinase reaction was stopped by adding SDS loading buffer, and the supernatants were subjected to a phosphate gel for immunoblotting to measure the in vitro phosphorylation reaction. Phosphate gel was 8% acrylamide gel with the addition of 5 mM Phos-tagTM (#034-93521(AAL-107)) and 10 mM Mn²⁺ in the resolving gel. Before transferring, the gel was washed 3 times every 10 min in the transfer buffer containing EDTA (10 mM), which is required to increase the transfer efficiency. Phos-tagTM and Mn²⁺ cooperates to bind a phosphorylated protein; when the phosphorylation levels are increased, the migration velocity of this protein is slower. Therefore, non-phosphorylated and phosphorylated proteins could be separated in the gel.

RNA isolation and qRT-PCR

Total RNA was extracted from cells or grated tissue in TRIzol (Takara), reverse transcribed with random hexamers (Sangon) and M-MLV transcriptase (Takara). qRT-PCR was performed to detect the mRNA levels of the indicated genes on a CFX-96 real-time PCR system (Bio-Rad) or LightCycler-480-384 (Roche) with SYBR Green Master Mix (Yeasen). qRT-PCR primer sequences are listed in Table EV2. β -Actin in human and mouse samples, or GAPDH in zebrafish samples were used to normalize gene expression. The “relative” mRNA levels were calculated using the $2^{-\Delta\Delta Ct}$ method with the normalized gene. The “fold” changes were calculated using the $2^{-\Delta\Delta Ct}$ method with the normalized gene and compared to the control groups including PBS, mock, WT mock, DMSO mock, siNC, Vector, PBS mock, WT siNC mock.

Statistics

Adequate power was ensured when choosing the sample sizes. Data are represented as the means of at least three experiments or representative of three independent experiments. Statistical analyses are performed using GraphPad Prism software, version 8. Statistical analysis was performed using unpaired or paired *t*-test or correlation or one-way ANOVA or two-way ANOVA test. The log-rank (Mantel-Cox) test is used for survival comparisons. ns, not significant ($P > 0.05$); * $P < 0.05$; ** $P < 0.01$; *** $P < 0.001$; **** $P < 0.0001$.

Data availability

This study includes no data deposited in external repositories.

Expanded View for this article is available online.

Acknowledgments

We thank Ming O. Li (MSKCC) and J. Ding (SIBCB, CAS) for providing kind advices and discussions and the Core Facility of Chemical Biology and Molecular Biology, Cellular Biology, and the Core Facility of Zebrafish

and the animal Facility. We thank the staff from the National Centre for Protein Science, Shanghai, especially Chao Peng, Yue Yin, and Chao-hua Zheng for their technological help with the MS analysis and mouse irradiation. This work was supported by Shanghai Municipal Science and Technology Major Project and grants from the Ministry of Science and Technology of China (2016YFD0500207, 2016YFD0500407), National Natural Science Foundation of China (32000631, 81930038, 81825011, 81630043 and 81961160738), China Postdoctoral Science Foundation (2020M671263), and the Strategic Priority Research Program of the Chinese Academy of Sciences (XDB19000000).

Author contributions

Hongyan Wang: Conceptualization; Resources; Supervision; Funding acquisition; Writing – original draft; Project administration; Writing – review and editing. **Xin Zheng:** Data curation; Writing – original draft; Writing – review and editing. **Jun Xiao:** Data curation; Investigation; Writing – original draft. **Qi Jiang:** Data curation; Investigation. **Lingming Zheng:** participated in part of the mice and zebrafish experiment. **Chang Liu:** participated in part of the mice and zebrafish experiment. **Chen Dong:** participated in part of the mice and zebrafish experiment. **Yuxiao Zheng:** participated in part of the mice and zebrafish experiment. **Peili Ni:** participated in part of the mice and zebrafish experiment. **Chi Zhang:** helped with experiments. **Fang Zhang:** Resources; helped with experiments. **Ruiyue Zhong:** helped with experiments. **Qiong Wang:** helped with experiments. **Ying Qiu:** helped with experiments. **Minxia Gao:** helped with experiments. **Bin Wei:** Funding acquisition; Writing – original draft; Writing – review and editing. **Huihua Ding:** Resources. **Jianping Ding:** providing kind advices and discussions, helped with experiments. **Nan Shen:** Resources.

In addition to the CRediT author contributions listed above, the contributions in detail are:

XZ performed the majority of experiments and analyzed data. JX, QJ, LZ, CL, CD, YZ, PN participated in part of the mice and zebrafish experiment. CZ, FZ, HD, RZ, QW, YQ, MG, JD, NS helped with experiments. XZ, HW and BW designed the study and wrote the paper.

Disclosure and competing interests statement

The authors declare that they have no conflict of interest.

References

- Aguilera-Pickens G, Abud-Mendoza C (2018) Pulmonary manifestations in systemic lupus erythematosus: pleural involvement, acute pneumonitis, chronic interstitial lung disease and diffuse alveolar hemorrhage. *Reumatol Clin* 14: 294–300
- Bengtsson AA, Ronnblom L (2017) Role of interferons in SLE. *Best Pract Res Clin Rheumatol* 31: 415–428
- Boxx GM, Cheng G (2016) The roles of type I interferon in bacterial infection. *Cell Host Microbe* 19: 760–769
- Celhar T, Magalhaes R, Fairhurst AM (2012) TLR7 and TLR9 in SLE: when sensing self goes wrong. *Immunol Res* 53: 58–77
- Chattopadhyay S, Kuzmanovic T, Zhang Y, Wetzel JL, Sen GC (2016) Ubiquitination of the transcription factor IRF-3 activates RIPA, the apoptotic pathway that protects mice from viral pathogenesis. *Immunity* 44: 1151–1161
- Chattopadhyay S, Sen GC (2017) RIG-I-like receptor-induced IRF3 mediated pathway of apoptosis (RIPA): a new antiviral pathway. *Protein Cell* 8: 165–168

- Coffer PJ, Woodgett JR (1991) Molecular cloning and characterisation of a novel putative protein-serine kinase related to the cAMP-dependent and protein kinase C families. *Eur J Biochem* 201: 475–481
- Dalskov L, Narita R, Andersen LL, Jensen N, Assil S, Kristensen K, Mikkelsen JG, Fujita T, Mogensen TH, Paludan SR et al (2020) Characterization of distinct molecular interactions responsible for IRF3 and IRF7 phosphorylation and subsequent dimerization. *Nucleic Acids Res* 48: 11421–11433
- Dummler B, Hemmings BA (2007) Physiological roles of PKB/Akt isoforms in development and disease. *Biochem Soc Trans* 35: 231–235
- Fayard E, Xue G, Parcellier A, Bozulic L, Hemmings BA (2010) Protein kinase B (PKB/Akt), a key mediator of the PI3K signaling pathway. *Curr Top Microbiol Immunol* 346: 31–56
- Fujita N, Sato S, Katayama K, Tsuruo T (2002) Akt-dependent phosphorylation of p27Kip1 promotes binding to 14-3-3 and cytoplasmic localization. *J Biol Chem* 277: 28706–28713
- Goropevsek A, Holcar M, Pahor A, Avcin T (2019) STAT signaling as a marker of SLE disease severity and implications for clinical therapy. *Autoimmun Rev* 18: 144–154
- Goulet M-L, Olagnier D, Xu Z, Paz S, Belgnaoui SM, Lafferty EI, Janelle V, Arguello M, Paquet M, Ghneim K et al (2013) Systems analysis of a RIG-I agonist inducing broad spectrum inhibition of virus infectivity. *PLoS Pathog* 9: e1003298
- Guerra-Varela J, Baz-Martinez M, Da Silva-Alvarez S, Losada AP, Quiroga M, Collado M, Rivas C, Sanchez L (2018) Susceptibility of zebrafish to vesicular stomatitis virus infection. *Zebrafish* 15: 124–132
- Honda K, Takaoka A, Taniguchi T (2006) Type I interferon [corrected] gene induction by the interferon regulatory factor family of transcription factors. *Immunity* 25: 349–360
- Huai W, Liu X, Wang C, Zhang Y, Chen X, Chen X, Xu S, Thomas T, Li N, Cao X (2019) KAT8 selectively inhibits antiviral immunity by acetylating IRF3. *J Exp Med* 216: 772–785
- Hubel P, Urban C, Bergant V, Schneider WM, Knauer B, Stukalov A, Scaturro P, Mann A, Brunotte L, Hoffmann HH et al (2019) A protein-interaction network of interferon-stimulated genes extends the innate immune system landscape. *Nat Immunol* 20: 493–502
- Jing T, Zhao B, Xu P, Gao X, Chi L, Han H, Sankaran B, Li P (2020) The structural basis of IRF-3 activation upon phosphorylation. *J Immunol* 205: 1886–1896
- Jordan MB, van Rooijen N, Izui S, Kappler J, Marrack P (2003) Liposomal clodronate as a novel agent for treating autoimmune hemolytic anemia in a mouse model. *Blood* 101: 594–601
- Kitamura T, Qian BZ, Pollard JW (2015) Immune cell promotion of metastasis. *Nat Rev Immunol* 15: 73–86
- Levy DE, Marie I, Smith E, Prakash A (2002) Enhancement and diversification of IFN induction by IRF-7-mediated positive feedback. *J Interferon Cytokine Res* 22: 87–93
- Li S, Zhu M, Pan R, Fang T, Cao Y-Y, Chen S, Zhao X, Lei C-Q, Guo L, Chen YU et al (2016) The tumor suppressor PTEN has a critical role in antiviral innate immunity. *Nat Immunol* 17: 241–249
- Lin R, Heylbroeck C, Pitha PM, Hiscott J (1998) Virus-dependent phosphorylation of the IRF-3 transcription factor regulates nuclear translocation, transactivation potential, and proteasome-mediated degradation. *Mol Cell Biol* 18: 2986–2996
- Lin R, Mamane Y, Hiscott J (1999) Structural and functional analysis of interferon regulatory factor 3: localization of the transactivation and autoinhibitory domains. *Mol Cell Biol* 19: 2465–2474
- Liu C, Xu X, Han L, Wan X, Zheng L, Li C, Liao Z, Xiao J, Zhong R, Zheng X et al (2020) LRCH1 deficiency enhances LAT signalosome formation and CD8(+) T cell responses against tumors and pathogens. *Proc Natl Acad Sci USA* 117: 19388–19398
- Lu Y, Qiu Y, Chen P, Chang H, Guo L, Zhang F, Ma Li, Zhang C, Zheng X, Xiao J et al (2019) ER-localized Hrd1 ubiquitinates and inactivates Usp15 to promote TLR4-induced inflammation during bacterial infection. *Nat Microbiol* 4: 2331–2346
- Maehama T, Dixon JE (1998) The tumor suppressor, PTEN/MMAC1, dephosphorylates the lipid second messenger, phosphatidylinositol 3,4,5-trisphosphate. *J Biol Chem* 273: 13375–13378
- Meng F, Zhou R, Wu S, Zhang Q, Jin Q, Zhou Y, Plouffe SW, Liu S, Song H, Xia Z et al (2016) Mst1 shuts off cytosolic antiviral defense through IRF3 phosphorylation. *Genes Dev* 30: 1086–1100
- Moro L, Arbini AA, Yao JL, di Sant'Agnes PA, Marra E, Greco M (2009) Mitochondrial DNA depletion in prostate epithelial cells promotes anoikis resistance and invasion through activation of PI3K/Akt2. *Cell Death Differ* 16: 571–583
- Morris R, Kershaw NJ, Babon JJ (2018) The molecular details of cytokine signaling via the JAK/STAT pathway. *Protein Sci* 27: 1984–2009
- Munier CC, Ottmann C, Perry MWD (2021) 14-3-3 modulation of the inflammatory response. *Pharmacol Res* 163: 105236
- Munz C, Lunemann JD, Getts MT, Miller SD (2009) Antiviral immune responses: triggers of or triggered by autoimmunity? *Nat Rev Immunol* 9: 246–258
- Ning S, Pagano JS, Barber GN (2011) IRF7: activation, regulation, modification and function. *Genes Immun* 12: 399–414
- Panne D, McWhirter SM, Maniatis T, Harrison SC (2007) Interferon regulatory factor 3 is regulated by a dual phosphorylation-dependent switch. *J Biol Chem* 282: 22816–22822
- Parker BS, Rautela J, Hertzog PJ (2016) Antitumour actions of interferons: implications for cancer therapy. *Nat Rev Cancer* 16: 131–144
- Reeves WH, Lee PY, Weinstein JS, Satoh M, Lu L (2009) Induction of autoimmunity by pristane and other naturally occurring hydrocarbons. *Trends Immunol* 30: 455–464
- Roy S, Bag AK, Dutta S, Polavaram NS, Islam R, Schellenburg S, Banwait J, Guda C, Ran S, Hollingsworth MA et al (2018) Macrophage-derived neuropilin-2 exhibits novel tumor-promoting functions. *Can Res* 78: 5600–5617
- Sadler AJ, Williams BR (2008) Interferon-inducible antiviral effectors. *Nat Rev Immunol* 8: 559–568.
- Saitoh T, Tun-Kyi A, Ryo A, Yamamoto M, Finn G, Fujita T, Akira S, Yamamoto N, Lu KP, Yamaoka S (2006) Negative regulation of interferon-regulatory factor 3-dependent innate antiviral response by the prolyl isomerase Pin1. *Nat Immunol* 7: 598–605
- Schneider WM, Chevillotte MD, Rice CM (2014) Interferon-stimulated genes: a complex web of host defenses. *Annu Rev Immunol* 32: 513–545
- Sekimoto T, Fukumoto M, Yoneda Y (2004) 14-3-3 suppresses the nuclear localization of threonine 157-phosphorylated p27(Kip1). *EMBO J* 23: 1934–1942
- Seo GJ, Yang A, Tan B, Kim S, Liang Q, Choi Y, Yuan W, Feng P, Park HS, Jung JU (2015) Akt kinase-mediated checkpoint of cGAS DNA sensing pathway. *Cell Rep* 13: 440–449
- Shiratsuchi H, Basson MD (2007) Akt2, but not Akt1 or Akt3 mediates pressure-stimulated serum-opsonized latex bead phagocytosis through activating mTOR and p70 S6 kinase. *J Cell Biochem* 102: 353–367
- Stambolic V, Suzuki A, de la Pompa JL, Brothers GM, Mirtsos C, Sasaki T, Ruland J, Penninger JM, Siderovski DP, Mak TW (1998) Negative regulation of PKB/Akt-dependent cell survival by the tumor suppressor PTEN. *Cell* 95: 29–39

- Taniguchi T, Ogasawara K, Takaoka A, Tanaka N (2001) IRF family of transcription factors as regulators of host defense. *Annu Rev Immunol* 19: 623–655
- Wang C, Wang Q, Xu X, Xie B, Zhao Y, Li N, Cao X (2017) The methyltransferase NSD3 promotes antiviral innate immunity via direct lysine methylation of IRF3. *J Exp Med* 214: 3597–3610
- Wu J, Chen ZJ (2014) Innate immune sensing and signaling of cytosolic nucleic acids. *Annu Rev Immunol* 32: 461–488
- Wu S, Zhang Q, Zhang F, Meng F, Liu S, Zhou R, Wu Q, Li X, Shen Li, Huang J et al (2019) HER2 recruits AKT1 to disrupt STING signalling and suppress antiviral defence and antitumour immunity. *Nat Cell Biol* 21: 1027–1040
- Xiao J, Li W, Zheng X, Qi L, Wang H, Zhang C, Wan X, Zheng Y, Zhong R, Zhou X et al (2020) Targeting 7-dehydrocholesterol reductase integrates cholesterol metabolism and IRF3 activation to eliminate infection. *Immunity* 52: 109–122
- Xie Y, Li J, Zhang C (2018) STAT3 promotes the proliferation and migration of hepatocellular carcinoma cells by regulating AKT2. *Oncol Lett* 15: 3333–3338
- Xue G, Zippelius A, Wicki A, Mandala M, Tang F, Massi D, Hemmings BA (2015) Integrated Akt/PKB signaling in immunomodulation and its potential role in cancer immunotherapy. *J Natl Cancer Inst* 107: djv171
- Xue S, Liu C, Sun X, Li W, Zhang C, Zhou X, Lu Y, Xiao J, Li C, Xu X et al (2016) TET3 Inhibits Type I IFN Production Independent of DNA Demethylation. *Cell Rep* 16: 1096–1105
- Yap TA, Walton MI, Hunter L-J, Valenti M, de Haven Brandon A, Eve PD, Ruddle R, Heaton SP, Henley A, Pickard L et al (2011) Preclinical pharmacology, antitumor activity, and development of pharmacodynamic markers for the novel, potent AKT inhibitor CCT128930. *Mol Cancer Ther* 10: 360–371
- Zhang B, Ma Y, Guo H, Sun B, Niu R, Ying G, Zhang N (2009) Akt2 is required for macrophage chemotaxis. *Eur J Immunol* 39: 894–901
- Zhang W, Wang G, Xu Z-G, Tu H, Hu F, Dai J, Chang Y, Chen Y, Lu Y, Zeng H et al (2019) Lactate Is a Natural Suppressor of RLR Signaling by Targeting MAVS. *Cell* 178: 176–189
- Zhang Y, Wang X, Yang H, Liu H, Lu Y, Han L, Liu G (2013) Kinase AKT controls innate immune cell development and function. *Immunology* 140: 143–152



License: This is an open access article under the terms of the Creative Commons Attribution-NonCommercial-NoDeriv 4.0 License, which permits use and distribution in any medium, provided the original work is properly cited, the use is non-commercial and no modifications or adaptations are made.